Faculty of Science and Technology
Department of Geology

UiT
THE ARCTIC
UNIVERSITY
OF NORWAY

Climate reconstruction during the Last Glacial Maximum based on a marine sediment core from Vestnesa Ridge, Svalbard

Felix Matteis

Master thesis in Geology (GEO-3900)
July 2018

Abstract

The sediment core HH15-1255PC has been analyzed to reconstruct the climate in the Fram Strait during the last 45,000 years. The coring site is located west of Svalbard on the Vestnesa Ridge, a contourite drift with a high-resolution sedimentary record (Plaza-Faverola et al., 2015). This ridge also includes a pockmark field formed by methane seepage (Vogt et al., 1994).

The core HH15-1255PC is a piston core, which was taken in the year 2015 at a water depth of 1,206 m. Onboard the magnetic susceptibility was measured and the core with its total length of 819 cm was cut into 9 sections.

In the laboratory of the University of Tromsø different measurements were done on the sediment core before parts of it were analyzed with destructible methods. These methods include core description, x-ray scans, XRF-core scanner, multi-sensor core logger and distribution analyses of foraminifera species.

Additionally, the oxygen/carbon isotopes were measured and five samples were used for radiocarbon dating. With the dating results, an age model was constructed by correlating the results with the core JM03-373PC2 described by Jessen et al. (2010). A debris flow deposit, which could be seen in both cores, gave an additional age mark.

By comparing the density curve for planktic foraminifera with the $\delta^{18}O$ results of the Greenland ice core, Dansgaard-Oeschger event 2 to 11 could correlated. As well, the curves for the detrital carbonate of the Deep Sea Drilling Project have been used and were compared with the 500 μm IRD fraction of the HH15-1255PC core to correlate Heinrich event 2, 3 and 4.

The results were put in relation with Dansgaard-Oeschger and Heinrich events and by analyzing the foraminifera distribution, it is possible to see how the influence of different water masses was changing during those events.

Acknowledgements

First of all, I would like to thank my supervisor Tine Lander Rasmussen for giving me the opportunity to work on this interesting project. She has been very helpful along the way and provided me with the material and information I needed for my thesis.

As well, I want to express my gratitude to all the help I received by the lab staff who has assisted me with my lab work and was always there if I had any questions. I was well introduced and made familiar with the equipment so that I could work efficient and effective. Thanks to Matteus Lindgren for doing the analysis for the stable isotopes.

In addition, my colleagues in the lab have been very helpful when I had specific questions.

Thanks to Mohamed Ezat for the assistance during the first half of my thesis.

Also I want to thank CAGE (Center for Arctic Gas Hydrate, Environment and Climate) for financing my carbon and isotope dating analysis.

Most of all, I want to thank my family back home who supported me during my studies and helped me to manage everything. They made it possible for me to come to Tromsø and study in this amazing place.

Table of Contents

List of Tables

List of Figures

1 Introduction

1.1 Objectives

The aim of this thesis is to study millennial scale oceanographic and climatic fluctuations in the Fram Strait by analyzing a marine sediment core.

The focus will be put on the investigation of the forcing behind Dansgaard-Oeschger and Heinrich events based on one piston core from the Svalbard margin. These climate variabilities occur cyclic and by the detailed analysis of those events, it is possible to gain better insight in both atmospheric and oceanic conditions in the Polar North Atlantic (Dokken et al., 1996).

The main objectives of this thesis are:

- The analysis of the foraminifera distribution
- The climate reconstruction of the last Weichselian glaciation
- Analysis of paleoclimatic and paleoceanographic processes in the Svalbard margin

1.2 Study area

The area of study is located in the Fram strait on the western shelf of Svalbard at 79°N. In this passage, water masses are flowing in and out from the Atlantic Ocean into the Arctic Ocean (Fig. 1). These ocean currents are the West Spitsbergen Current, which is transporting warm, saline water northwards (Bourke et al., 1988), and the colder and low-saline East Greenland Current (Aagaard et al., 1968). At this specific location, the heat flow of the Arctic Ocean takes place by the exchange of warm Atlantic water and cold polar water (Schauer et al., 2004). Also during the Holocene, the meltwater of the glaciers played an important role (Rasmussen, 2013). As illustrated in figure 2, the coring site is located close to where both the West Spitsbergen Current and East Spitsbergen Current are flowing. Due to changes in glacier advance and sea ice distribution, the ocean currents can vary and influence marine setting and sedimentation rate.

The sediment core was taken from a pockmark on the Vestnesa Ridge. This ridge can be identified as a contourite drift, since this oceanic feature was formed as sediment was transported and deposited through ocean currents along the Svalbard continental shelf.

A contourite drift is characterized by a high sedimentation rate, which provides a sedimentary record on a time-scale that makes it possible to see Dansgaard-Oeschger and Heinrich events

(Plaza-Faverola et al., 2015). Additionally, the Vestnesa Ridge is covered by a large pockmark field that was formed by methane seepage from the ocean floor (Vogt et al., 1994).

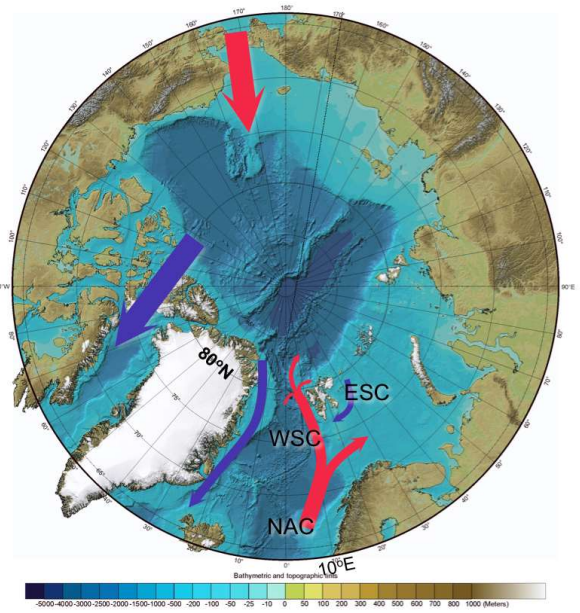

Figure 1: *A map illustrating the North Atlantic Current (NAC), West Spitsbergen Current (WSC), and East Spitsbergen Current (ESC) (bouwmadesign.com, 2018. Arctic Biogeochemistry)*

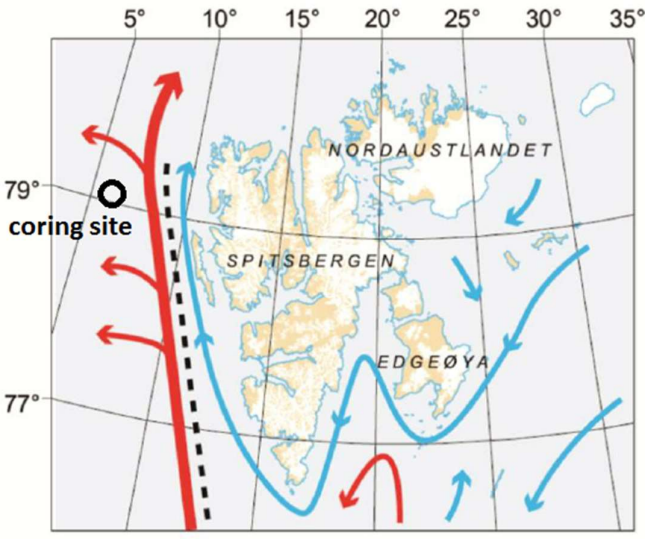

Figure 2: *Modified map showing the coring site with the West Spitsbergen Current (red) and East Spitsbergen Current (blue) (Przybylak et al. 2012)*

1.3 Oceanography

1.3.1 Ocean currents

Ocean currents in general play an important role in the world's ocean and can have a big influence on the climate. The so-called thermohaline circulation is the global transport mechanism of water masses, which connects all oceans with each other. The origin for that natural phenomenon is the difference in temperature and salinity (Broeker, 1997).
In the North Atlantic, warmer water is flowing northwards on the surface of the ocean. These water masses are directly exposed to the atmosphere. Close to the Greenland ice sheet, those water masses are cooling down and loosing buoyancy. As a result of this process, the North Atlantic Deep water (NADW) is flowing southward on the ocean floor. By combining those two currents and taking the overturning process of water masses under consideration, this circulation can be described as the Atlantic Meridional Ocean Circulation (McManus et al., 2004)

For the heat transport in the North Atlantic, this circulation plays an important role (Lynch-Stieglitz et al., 2018).
The direction of the water current is also defined by the general bathymetry of the North Atlantic. The Greenland basin, which is surrounded by ridges and continental shelves, contains North Atlantic Bottom Water. This bottom water is also described as overflow water, since it is formed by dense water masses flowing over the Greenland-Scotland ridge.
Between the surface water and deep water, the intermediate water masses are located (Hopkins, 1991).
The climate in the North Atlantic and especially in the Fram strait is highly controlled by the West Spitsbergen Current (WSC) (Fig. 3), a current linked to the Norwegian Atlantic Current. Relatively warm water from the North Atlantic is transported in the Arctic, which causes that the Fram Strait is the northernmost permanently ice-free ocean on our planet (Haugan, 1999).

Compared to the West Spitsbergen Current, which transports warm water and flows northward, there is the East Greenland Current on the western side of the Framstrait. This ocean current transports cold water from the Arctic Ocean into the North Atlantic. Since those water masses

are much colder, they are also denser and therefore flowing on the ocean floor (Rudels et al., 2002).

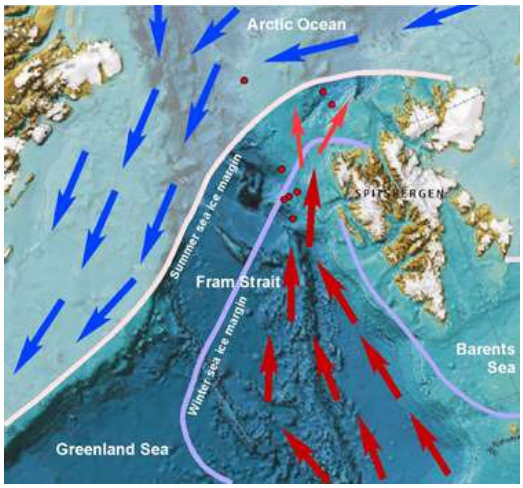

Figure 3: *Illustration of the West Spitsbergen Current and East Greenland Current (geo.uni-bremen.de, 2017. Holocene variability in the Arctic gateway)*

The other important ocean current in the study area is the East Spitsbergen Current. With similar characteristics like the East Greenland current, this current is transporting cold and dense water from the north-eastern side of Svalbard in a clockwise pattern around the southern tip of the archipelago and northwards along the shelf (Quadfasel et al., 1988).
At the coring site, the Vestnesa ridge is mainly under influence of the West Spitsbergen Current (Bünz et al., 2012).

1.4 Dansgaard-Oeschger events

For a better understanding of Quaternary climate fluctuations, the Greenland ice core project (GISP) played an important role. During this project, two deep ice cores with a length of 3,027 m and 3,053 m were drilled into the ice sheet (Fig. 4). By measuring the $\delta^{18}O$ values along the core, it is possible to see climate fluctuations back to 105,000 years before present.

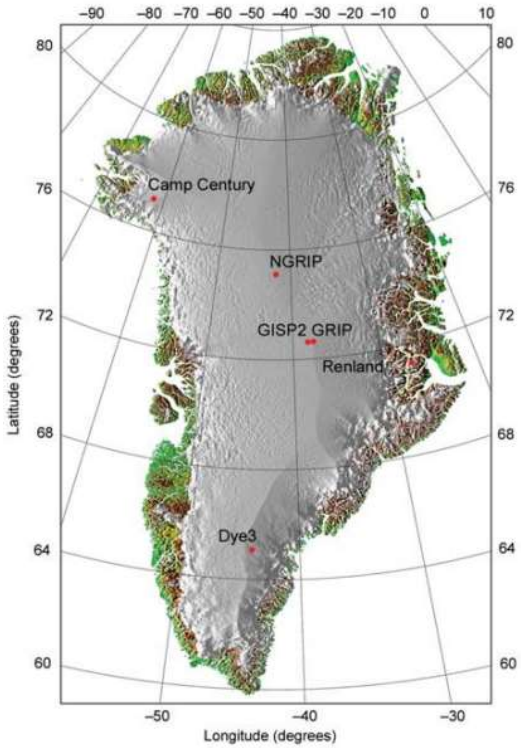

Figure 4: *Location of the ice core drilling sites - GRIP (72.5 8°N, 37.3 8°W), GISP2 (72.5 8°N, 38.3 8°W), NGRIP (75.1 8°N, 42.3 8°W) (Andersen et al., 2004)*

These oxygen isotope values show 24 distinct temperature changes during this period, which were named as Dansgaard-Oeschger events (Andersen et al., 2004).

Dansgaard-Oeschger events are defined as rapid climate fluctuations during the last glacial period. More precisely they consist of interstadials, warm periods, followed by stadials, cold periods (Andersen et al., 2004). The warming occurs very rapid, whereas the cooling phase is relatively slow. The Dansgaard-Oeschger events usually last over a period of 1,000 to 3,000 years (Cacho et al., 1999). In the timeframe that the Greenland Ice core covers, 25 of such events are known (Andersen et al., 2004).

The reason behind Dansgaard-Oeschger events is not completely understood, but a plausible reason behind their occurrence could be due to changes in solar activity (Braun et al., 2005).

As stated by Andersen et al. (2004), the oxygen isotope values in sediment cores follow a very similar pattern as the ice cores (Fig. 5), which allows to correlate the Greenland Ice core to various marine cores from the North Atlantic.

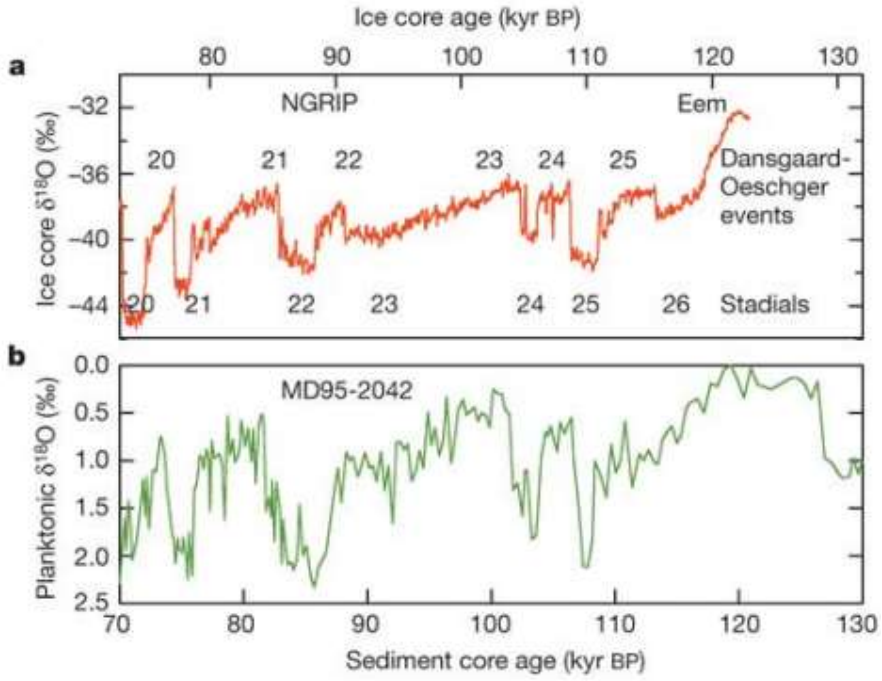

Figure 5: *Oxygen isotopes from the NGRIP compared to planktonic isotopes from a core in the Iberian margin (Andersen et al., 2004)*

1.5 Heinrich events

First described by Heinrich in 1988, Heinrich events are periods where a large amount of ice-rafted sediment is deposited on the ocean floor. During the last glacial period, the Northern Hemisphere was covered with huge ice sheets. That also means that there was a lot of discharge of drift ice into the ocean. These icebergs carry large amounts of sediment, which have been eroded by glacial activity. When the icebergs melt, this material drops on the seabed (Hemming, 2004). Since icebergs can drift over quite big distances, layers of ice rafted debris (IRD) can be found all over the North Atlantic (Fig. 6). These layers of ice rafted debris are described as Heinrich layers. Their thickness can be interpreted as how strong the melting event was and their distribution shows how the ocean current transported the material over the Atlantic (Dowdeswell, 1995). The main deposition area of IRD is located at a latitude of 47° to 51° N. That is due to the fact that it is in this area where most of the icebergs are melting (Ruddiman, 1997).

As a conclusion, Heinrich events represent surges of the ice sheets, which filled the North Atlantic with icebergs. In total, there are six of such Heinrich events known. They are described as H1 to H6, from youngest to oldest (Broecker et al., 1991).

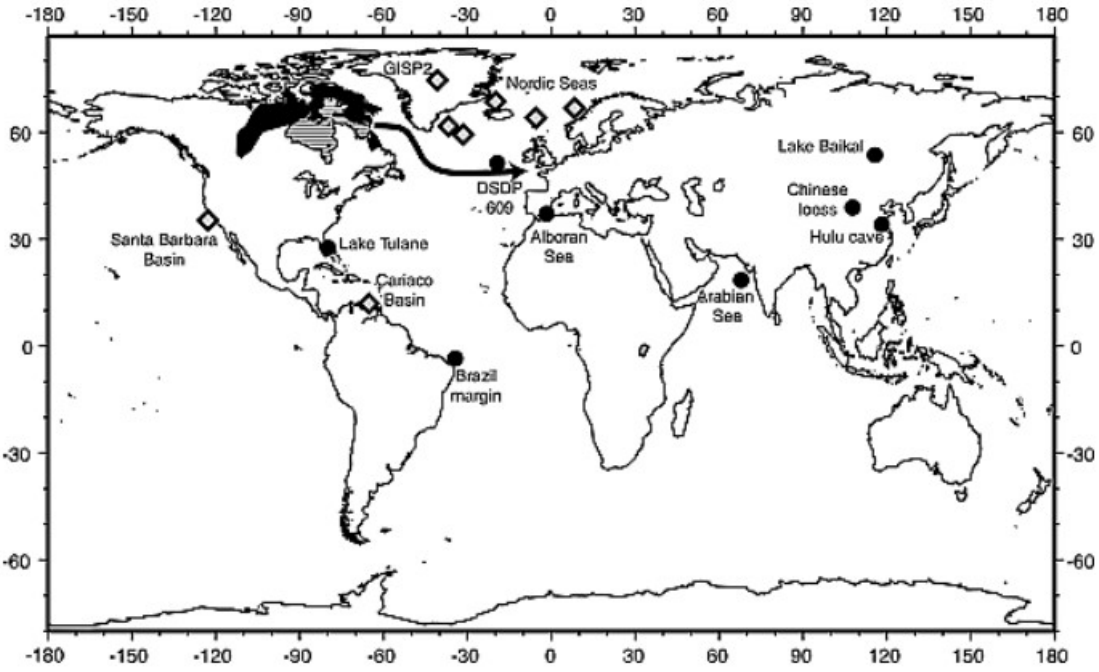

Figure 6: *Illustration showing the origin and transport path of Heinrich events (Hemming, 2004)*

As noted by Bond et al. (1993), Heinrich-events are closely linked to Dansgaard-Oeschger cycles. There are different explanations and models for the occurrence of Heinrich events, but all theories are based on the growth and decay of large ice sheets and its connection with the ocean currents. Large ice sheets can have a big influence on ocean currents and by releasing freshwater, they can slow down ocean circulation (Bond et al., 1993).

1.6 Foraminifera

Foraminifera are a very abundant group of single-celled protozoa. They have been present since the Cambrian at around 560 million years ago through to present time. This group reached its peak during the Cenozoic.
Foraminifera make up 55 % of the Arctic biomass and over 90 % of deep sea biomass.
Depending on their habitat, they are generally classified as planktic and benthic foraminifera. They are either living in the water column in a planktonic state or on the sea bed.
What makes the different foraminifera species so characteristic is their shell, which consists either of minerals or of agglutinated particles. The shell can be described by the amount of chambers and the location of the opening of the shell (Armstrong, 2009).
The different foraminifera species are well adapted to specific climate conditions and can be used to reconstruct paleoenvironments.

1.6.1 Planktic foraminifera

Planktic foraminifera produce a calcareous shell. There are only 50 known species, but they are present in all parts of the Global Ocean, from the tropics to the polar regions and make up an enormous biomass. There are more different species in the tropics and subtropics than in polar waters. Most of them are living in surface water below the wave base to up to 1,000 m.
Their shells reflect the characteristics of the waters they were calcified in and can be used as an indicator of ocean currents and worldwide climate changes, since the species is directly linked with salinity and water temperature. After death, they sink to the ocean floor and are preserved in the sediment (Ohtsuka et al., 2015).

The left coiling *Neogloboquadrina pachyderma* (Ehrenberg, 1861) is a common polar species (Darling et al., 2006). The distribution of this species is closely linked to the availability of chlorophyll being its main food source. That is the reason for that the highest density of *N. pachyderma* is located at a water depth between 20 and 80 m (Kohfeld and Fairbanks, 1996).

Neogloboquadrina incompta (Cifelli, 1961) is described by Darling et al. (2006) as a morphospecies of *Neogloboquadrina pachyderma. Neogloboquadrina incompta* is right coiling

and common in subpolar water masses. The ration between this two species can be used to differentiate polar from subpolar water.

Turbototalia quinqueloba (Natland, 1938) can be found in warmer Atlantic water masses at a depth from 30 – 70 m (Schäfer et al., 2001).

Globigerina bulloides (Brady, 1881) is a species that is common in sub-polar water and in areas where upwelling occurs (Spero and Lea, 1995).

1.6.2 Benthic Foraminifera

Benthic foraminifera are present in all deep sea environments (Corliss, 1984). They are living at the ocean floor and in the sediment. Just like planktic foraminifera, there are both agglutinated and calcareous species. Since agglutinated species break apart very easily after they die, it is not possible to find them in many fossil records. The shell from calcareous species is often preserved and therefore suitable for Quaternary stratigraphy (Corliss, 1984).
By analysing their shell, it is possible to extract important information about how the climate changed throughout the glacial and interglacial periods (Mackensen et al., 1985).

Cassidulina neoteretis (Seidenkrantz, 1995) is a benthic species that can be found in areas where there is both Atlantic and Polar water (Andrews and Dunhill, 2003).

Melonis barleeanus (Williamson, 1858) is an infaunal species, that shows abundance in soils with a high nutrient concentration (Elberling et al., 2002).

Stainforthia loeblichi (Feyling-Hanssen, 1954) is a common arctic species and associated with cold polar water (Knudsen, 1984).

Quinqueloculina seminula (Linnaeus, 1758) can be found in tidal-dominated environments (Hayward, 1981)

2 Material and Methods

The sediment core HH15-1255PC was taken in the year 2015 during a cruise along the western shelf of Svalbard. The exact position of the coring site is 79°00'57"0 N and 6°54'52"5 E at a water depth of 1,206 m (Fig. 2). The core has a total length of 8.19 m and was cut into 9 sections. Later on in the lab of the University of Tromsø different methods have been used to analyze the core. The aim of those methods is to show distinct parameters of the sediment core, which can be correlated to past events.

2.1 Coring

The coring took place on board of the research vessel Helmer Hanssen. This ship was built in 1988 and first used as a stern trawler for the fishing industry. Later on in 1992 the ship was rebuild as a research vessel. The University of Tromsø owns the ship since 2011. The main research areas of this vessel is the Norwegian Sea, the Barent Sea and parts of the Arctic Ocean around Svalbard (uit.no, 2017. FF Helmar Hanssen).

The core was taken with a piston corer (Fig. 7), which is installed on deck of the ship. The principle behind a piston corer is very similar to the gravity core. First of all, after the core is released the gravitational force is accelerating the core. Just before the core hits the sea floor, a piston mechanism is triggered and shots the core into the sediment. This allows the core to penetrate deeper in the sediment so that material from the end of the last ice age can be extracted.

A piston corer consists of different modules. At the lower end of the core, a core cutter is installed. This is the part of the core, which can penetrate through the sediment. A core catcher allows the sediment to enter the core tube in one direction, but not in the other.

The sediment is caught inside a plastic tube, which can be inserted and later be detached. On top of the core tube, there is a weight, which accelerates the core and provides stability against ocean currents and movements of the boat (Nesje, 1992).

After the drilling is executed, the plastic tube is pulled out on deck of the ship and cut into 1 m sections. Afterwards, the shorter pieces are cut, labeled and sealed.

Onboard the magnetic susceptibility was measured by pushing the core through a loop sensor. The core was then stored unopened onboard of the ship and kept cool at 4°C.

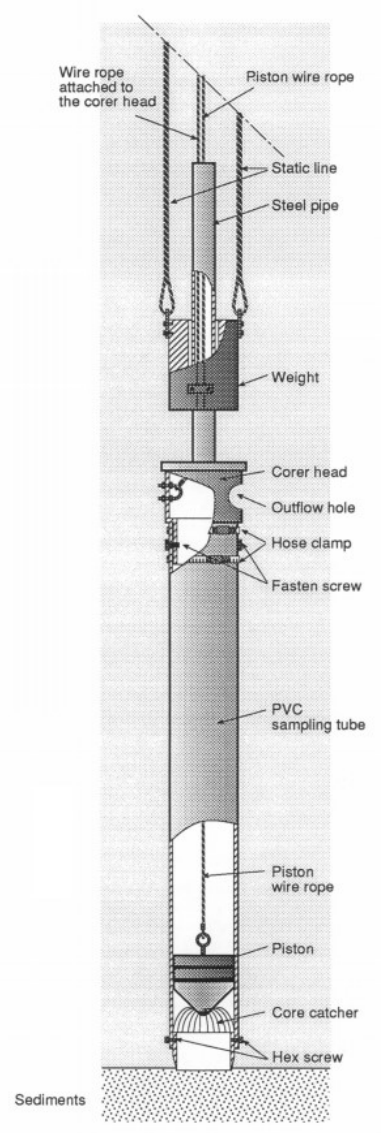

Figure 7: *Internal composition of a piston corer (Nesje, 1992)*

2.2 Measurements in the laboratory on the unopened core

2.2.1 Core X-Ray

The instrument, which is used at the University of Tromsø, is a Geotek x-ray core imaging system (Fig. 8). This method is used before the core is opened to get a first glimpse about the inside of the core. It gives information about lithology, bioturbation and ice-rafted debris.
The different cores were put on a conveyor belt on one side of the machine. Afterwards, the whole machine was closed so that the radiation around the machine is reduced to its minimum. Then the core gets pushed through the machine, is being x-rayed and the data is sent to a computer. On the other side of the machine, the core can be taken out again and another one can be scanned. The whole processs for one core only takes a few minutes (uit.no, 2017. X-Ray Instrument).

Figure 8: *Geotek x-ray core imagine system at the University of Tromsø (uit.no, 2018. X-Ray instrument)*

2.3 Opening of the core

The core was opened on the 19th April 2017 with a core liner saw by being pushed along two vibrating saws that sit on each side of the core (uit.no, 2017. Core Liner Saw) (Fig. 9).
This cuts the hard plastic on the side, but the sealed cap still need to to be opened on each end. Afterwards those caps were cut with a carpet knife.
Now to completely open the core and split the sediment in the inside, an electro-osmotic knife is used. This is connected to an electric current, which reduces the resistance when the core is opened (McMillen, 1977).

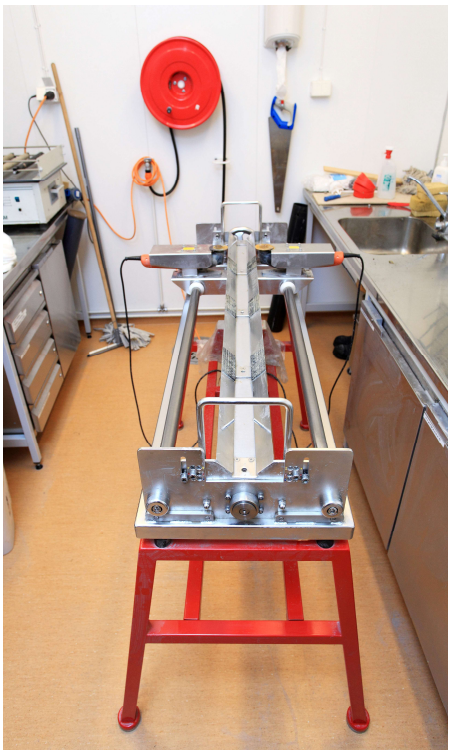

Figure 9: *Core Liner Saw at the University of Tromsø (uit.no, 2018. Core Liner Saw)*

After the core is split, it is important to label each half with name, section number and where the top and bottom end is located.
Depending on which half has more material, contains more shell fragments and has a cleaner cut, one half will be used to work on, the other one is stored as an archive for back-up.
The working section was cleaned with a plastic card to provide a clean surface without any disturbances. This process is needed before scanning the core with the XRF core scanner.
Afterwards, both cores were wrapped in plastic foil. The archive cores were as well sealed in plastic bags to be more protected. Afterwards, the cores are stored in a cooling room.
As the cores were opened, a strong smell was noticeable. This is due to the fact that they contain a lot of methane. The sediment of the Vestnesa Ridge is rich in pore fluids and gases (Vogt et al., 1994). When sediment is extracted from the seabed, methane gas is trapped inside the core. Some of the cores are almost empty or have large gaps with no sediment. This is because methane expands when being transported from the ocean floor to atmospheric pressure. The gaps in the core are most likely not missing parts but where the sediment was pushed apart by expanding methane.

2.4 Measurements in the laboratory on the opened core

2.4.1 XRF core scanner

The Avaatech XRF (x-ray fluorescence) core scanner is a fast and efficient method to analyze the elementary content of a marine sediment core.

The principle behind is the use of radiation with a short wave length (x-ray). This ionizes electrons and if the energy is high enough, an electron is kicked out of the atom. Another atom from a higher electron shell is falling back and emitting a characteristic radiation. There is a certain radiation for each element and by looking at the energy of the radiation, it is possible to determine the specific elements (Richter et al., 2006).

The XRF Core scanner at the University of Tromsø (Fig. 10) is installed in a 20-feet container, which allows transportation and the usage on scientific cruises. The scanner has a sample resolution of 1 cm within 30 minutes and scanning a whole core can be done within 30 min. That is about the time it takes for the whole coring process, including cutting the core into shorter pieces and sealing therm. That makes it possible to take XRF measurements in-between coring time.

This core scanner also has a core fit system, which allows fine adjustment of the core (uit.no, 2018. XRF core scanner container lab).

For analyzing HH15-1255PC, the x-ray radiation was turned off and only the scanner was used to take images from the core surface.

Figure 10: *XRF core scanner container lab at the University of Tromsø (uit.no, 2018. XRF core scanner container lab)*

2.4.2 Multi-Sensor Core Logger

The Multi-Sensor Core Logger (MSCL) (Fig. 11) is a variable usable machine, which can measure the
wet-bulk density, p-wave velocity and amplitude, magnetic susceptibility and temperature in sediment and rock cores. It also gives a colour code along the core.
The magnetic susceptibility measures to which degree a material can be magnetified while a strong magnetic field is created on the core surface. The machine measures to which extent the material is responding to the magnetic field (Weber et al., 1996).
The Multi-Sensor Core Logger pushes the core along a point sensor and makes a measurement at every cm. The sensor will just slightly be pressed into the sediment leaving push marks. Those marks can easily be removed by scraping with a plastic card over the sediment surface.

Figure 11: *MSCL at the University of Tromsø (uit.no, 2018. MSCL with spectrophotometer)*

2.5 Sample preparation

By looking at the logs and the magnetic susceptibility results, it was decided that samples are taken from 300 – 700 cm.

First of all, the core was cut into 1 cm pieces, which were packed into plastic bags and labeled. The sediment inside the plastic bag was pushed to the bottom to increase the contact area with the sediment and the plate in the freeze dryer.

Those bags were then weighted and put in the freezer for 24 hours. It is important to mention that several plastic bags have been weighted to calculate an average for the bag. The weight of the sediment can be calculated by subtracting the weight of the bag from the total weight.

Afterwards, the samples were put in the freeze dryer for another 24 hours. The principle behind the freeze dryer is that a vacuum is created and the plate, where the samples are lying, is heated. At such a low pressure the ice goes directly into vapor (Fig. 12) leaving behind a dry sample. After freeze-drying, the samples were weighted again to see how much water the sediment contained.

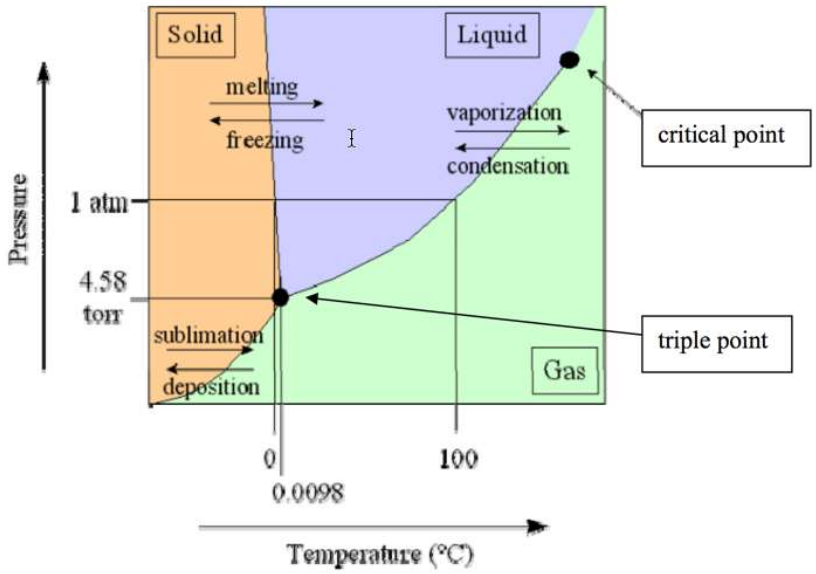

Figure 12: *Graph showing at which pressure and temperature freeze drying is possible (spscientific.com, 2018.Basic Principles of Freeze Drying)*

2.6 Sieving

To extract foraminifera, the samples need to be sieved. For achieving a high time resolution, every third sample was sieved.

The samples were put on top of four sieves with different mash sizes of 63 µm, 100 µm, 500 µm and 1 mm. Afterwards, the samples were wet sieved so that the sediment can sink through the different sieves. The residues of the 63 µm, 100 µm section were dryed in an oven at 40°C. Residues with larger grain size were dryed on a heating plate.

The residues from each sample were kept, even though only the 100 µm and 500 µm sections are used afterwards. Most of the forams are expected to be in the 100 µm section. The 500 µm section is used to analyze larger forams and Ice Rafted Debris.

The 63 µm and 100 µm fraction was put in a filter paper. After that, the filter was closed with a paper clip and put in an oven at 40 °C for one day. The dryed samples were then put in small glass jars.

The 500 µm and 1 mm fraction was put in a glass bowl and heated on a heating plate so that the water evaporates. Afterwards, those fractions were put in plastic bags.

2.7 Analysis of foraminifera

Most of the foraminifera are found in the 100 µm fraction. The analysis was done at every third cm in the core. This is considered a resolution, which can combine both accuracy and the limited time which was planned for the lab work.

To analyze the distribution of foraminifera, they need to be picked under a microscope and collected in slides.

When the sample was too large, the sample was split with a micro splitter. The principle behind it is that, when the sediment is put into the core splitter, half of the sediment falls on one tray, the other half on another tray.

The sample was spread evenly on a tray, which contains 45 squares. The foraminifera were counted and picked in random squares until those squares were empty. A total amount of 300 planktic foraminifera were picked.

The benthic foraminifera were not as abundant as planktic foraminifera. In many samples there was only a maximum of 50 to 100 individuals. While picking, the number of species was

counted and how many squares were used. With this information and the weight of the sample, the foraminifera density could be calculated.

2.8 Foraminifera density

After the foraminifera in each sample were counted, the density of both planktic and benthic species could be calculated.

The foraminifera density describes the number of individuals per gram dry weight. The foraminifera were counted in a tray with 45 squares and picked until a certain number of foraminifera was collected. The amount of squares, which was needed to collect a sufficient amount of foraminifera was noted. The density of foraminifera was calculated with the following formula:

$$\frac{Number\ of\ Planktic\ forams * \left(\frac{45}{Squares\ counted}\right)}{total\ dry\ weight}$$

2.9 Radiocarbon dating

Radiocarbon dating is a method to define the age of a sample by measuring the ^{14}C content. There are three different carbon isotopes with different abundance: ^{12}C (98.9 %), ^{13}C (1.1 %) and ^{14}C (10-14 %). For the radiocarbon dating method, the amount of ^{14}C is measured.

When the organism is still alive, there is an exchange with the carbon isotopes, so that the amount of ^{14}C is stable. There is always ^{14}C decay and intake at the same time. ^{14}C is formed in the atmosphere as cosmic radiation creates neutrons, which collide with ^{14}N atoms and produce ^{14}C (Bowman, 1990).

^{14}C is relatively unstable and is decaying with a half-life of 5,730 years to ^{14}N and other stable carbon isotopes (Bard et al., 1990).

Due to the constant radiation, the amount of ^{14}C in the atmosphere is relatively stable. Organisms who have an intake of carbon will also have a certain intake and storage of ^{14}C in their body.

When the organism dies, the ^{14}C intake stops and the amount of ^{14}C, which is in the organism, starts to decay. By measuring the amount of ^{14}C that is still left after it decayed over time, the age can be measured with some uncertainties (Bowman, 1990).

Figure 13 shows how far back in time the ^{14}C dating is possible. At around 20,000 years, the amount of carbon is only 10% of the carbon from the start. At an age of close to 30,000 years only a few percentage of carbon is left and ^{14}C dating is no longer possible. Other dating methods need to be used for older samples. The samples from the HH15-1255PC core were expected to be younger than that age. Therefore ^{14}C dating is considered as a suitable method.

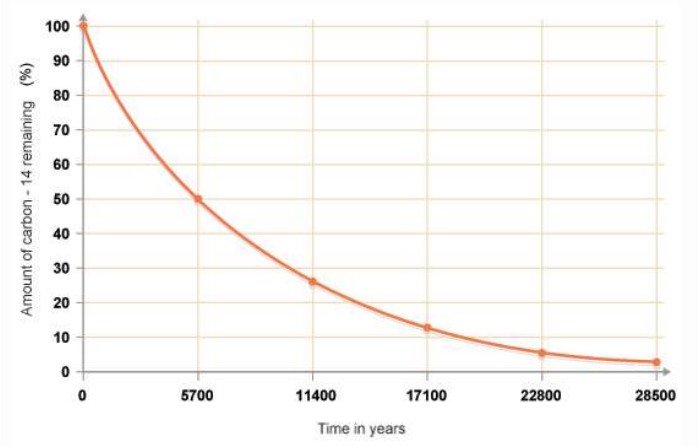

Figure 13: *A graph showing the decay of ^{14}C over time (thatslifesci.com, 2016. Estimating the Age of Life Long-Gone)*

To construct an age model, five samples have been sent to the ^{14}CHRONO Centre laboratory in Belfast, Ireland for radiocarbon dating.

To choose which of the samples were taken, the curve for the density of planktic foraminifera was used. This is to make sure that foraminifera are collected from samples which contain enough specimens. To get accurate results for the radiocarbon dating, a certain amount of material is needed. For each of the samples an amount of 1,200 *Neogloboquadrina pachyderma* was picked. Sample number 1, 2, 3 and 5 only contain foraminifera, whereas sample number 4 consists of fragments of one single shell. The shell was relative big, so that a few pieces were enough to reach the needed amount of material.

The radiocarbon ages differ from real ages and must be converted to "calendar years". The reason for this is, that the ratio between $^{14}C/^{12}C$ is not constant over time (Talma and Vogel, 1993). The ages were calibrated with the software CALIB Radiocarbon Calibration 7.1. The software calculates the calendar age before present (calBC) with an uncertainty of a few hundred years. The Calendric age before present represents the age before 1950. After that time, the test of nuclear bombs added too much ^{14}C to the atmosphere (Spalding et al., 2005).

However, before putting the ages in the software, the reservoir age of the samples needs to be considered in the calculation. The reservoir effect originates from the different ages of seawater. Theoretically, the amount of ^{14}C in the ocean should be in balance with the atmosphere, but the exchange of carbon only happens at the surface. Big water masses circulate relatively slowly so that the amount of ^{14}C already starts to decay when there is no longer any direct contact to the atmosphere. The foraminifera and shells use this carbon to build their shells (Bard et al., 1988). Depending on the location, samples have a different reservoir age. For the Fram Strait a reservoir correction of 440 years needs to be done before calculating the calendric age (Jones and Keigwin, 1988).

With the real ages and the distance between the samples in the core, the sedimentation rate can be calculated.

Later on, when certain peaks have been identified and are correlated to events, the age model can be adjusted.

2.10 Measuring oxygen and carbon isotopes

Another useful method is the measuring of stable oxygen and carbon isotopes.
For oxygen, the stable isotopes are ^{16}O and ^{18}O, which make up 99.759 % and 0.204 % of the total oxygen. The stable isotopes of carbon are ^{12}C and ^{13}C. By looking at the total amount of carbon, ^{12}C is 98.89 % and ^{13}C 1.11 % (Rundel et al., 1989).
The ratio between the different isotopes is being measured and compared to a standard. The calculated values are expressed in $\delta^{18}O$ and $\delta^{13}C$.
The standards are used internationally for comparable results. It is important to know that there are different standards in use. The most known ones are the PeeDee Belemnite (PDB), the standard for carbon and oxygen and the Standard Mean Ocean Water (SMOW), which is the standard for hydrogen and oxygen (Rundel et al., 1989).

For calculating $\delta\,^{18}O$ and $\delta\,^{13}C$ values following formulas are used (Sherwood Lollar et al., 1999):

$$\delta^{18}O = \frac{^{18}O/^{16}O_{sample} - ^{18}O/^{16}O_{standard}}{^{18}O/^{16}O_{standard}} \times 1000$$

$$\delta^{13}C = \frac{^{13}C/^{12}C_{sample} - ^{13}C/^{12}C_{standard}}{^{13}C/^{12}C_{standard}} \times 1000$$

Those values are measured in concentration units per thousand relatively to the standard.
A foraminifera shell will build oxygen and carbon isotopes in the shell depending on the surrounding seawater (Fig. 14) where the shell calcifies. The isotope relations in the seawater are depending on different parameters. The most important one is how much water is stored in ice on land, which influences the global amount of $\delta^{18}O$. Besides that, the temperature and salinity are effecting the $\delta^{18}O$ values. By measuring oxygen isotopes, the climate can be reconstructed (Grootes et al., 1993).

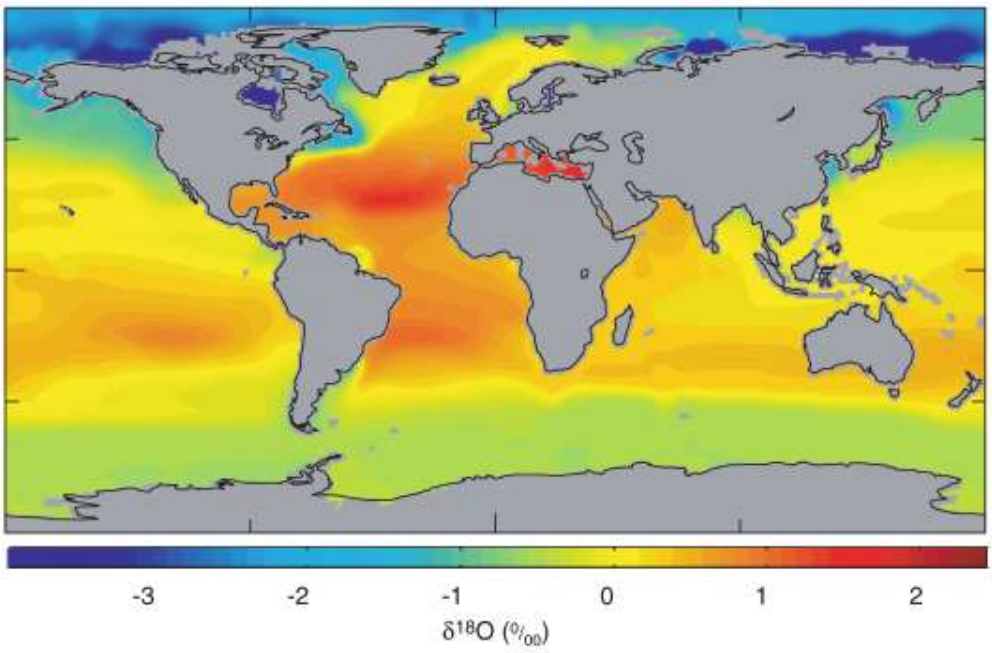

Figure 14: *Map showing the global seawater $\delta^{18}O$ of the ocean (data.giss.nasa.gov, 2018. Global Seawater $\delta^{18}O$ Database)*

There also is the so called "Vital effect". That means that different foraminifera species are building in different values of $\delta^{18}O$. This has to be considered when the isotope values are measured and compared with each other (Ravelo and Hillaire-Marcel, 2007).

The isotopes have been measured in the Stable Isotope Laboratory (SIL) at the Department of Geosciences at the University of Tromsø. This laboratory is part of CAGE, the Center for Arctic Gas Hydrate, Environment and Climate.

The amount of $\delta^{13}C$ and $\delta^{18}O$ has been measured with a Thermo-Fisher MAT253 isotope-ratio mass spectrometer with a Gasbench II (Fig. 15). The analyzed samples from the core were solid, but measurements can also be done on liquids.

Samples were taken from the sediment core from 300 to 700 cm at every 6th cm. To analyze the samples they have been put in 4.5 ml vials.

In the lab there was no pre-treatment done on the samples. Before the samples were put into the machine, the vials were exposed with helium and five drops of water free H_3PO_4 were added. Afterwards, the samples were equilibrated at 50°C for more than two hours and analyzed by the Gasbench II and the MAT253 isotope-ratio mass spectrometer. The measurements were normalized by the international standard VPDB, the Pee Dee Belemnite (Analysis report – Appendix, 2018).

Figure 15: *Isotope spectrometer at the University of Tromsø (uit.no, 2016. Stable Isotope Laboratory)*

2.11 Ice Rafted Debris

Ice rafted debris origins from terrestrial sediments, which is transported on top and within floating ice. This material can be transported over a long distance. The sediment is released and drops to the ocean floor when the ice melts. Icebergs can travel a long distance before they melt and release the sediment.

During glacial periods and in areas, which are characterized by floating icebergs and sea ice, there will always be some release of IRD. But only periods with immense iceberg discharges, will result in distinct layers of IRD on the ocean floor. These periods are described as Heinrich events (Hemming, 2004).

To analyze the glacial activity and to determine at which parts of the core Heinrich events happened, the IRD in the 500 μm and 1 mm fraction of the HH15-1255-PC core was counted. The samples was evenly spread over a tray and the grains were counted under a microscope. Afterwards, the number of counted IRD was divided by the weight of the sample to calculate the amount of IRD per gram. For the bigger fraction, it was possible to count the IRD with the naked eye. It was important to check with a metal pin if the grains are real IRD. Some of them looked like IRD, but were just compacted sediment and easy to destroy.

3 Results

In this chapter, the results from the lab work on the core HH15-1255PC will be presented in the same order as they were introduced in the introduction section.
First of all, the core description (Fig. 16) will give a general information about the core. After that, the x-ray images, magnetic susceptibility, foraminifera analysis, dating results, isotope measurements and IRD analysis will be described.
The results will give profound information for the core, which are distinct for its location in the Fram Strait.

3.1 Core description – logs and scans

The core HH15-1255PC was cut into one-meter sections, with the exception that the third section is 60 cm and the forth section 50 cm long.
Since the first section is missing, there is no direct information about the youngest sediment except from the onboard logging of the magnetic susceptibility (Fig. 17).
The second section is relatively uniform. It is fine laminated with parallel greyish and darker layers. The first 20 to 30 cm feel wet. There is also a distinct lighter grey layer at 133 to 140 cm. This layer contains slightly more coarse material. Most of the core consists of clay, whereas this layer is out of fine sand. The lower part of this fraction is layered, but the layers are slightly wavy and more spotted.
The third core only measures 60 cm. The upper 50 cm are very similar to the lower part of the previous core, but with a few more lamina. There is a distinct boundary at around 248 cm where the sediment is changing from brown to a grey colour. A bigger shell was found at 258 cm.
The forth core also contains grey sediment like the last 10 cm of the third core, as well as shell fragments and lighter spots.
In the lower part of the core, there are large pieces of authigenic carbonate. This mineral is formed at methane seeps as bacteria are oxidizing the gas. As a result of this process, CO_2 gets released, carbonate is precipitated and crusts are formed (Pierre, 2007).

A relatively large red-brown layer from 368 to 398 cm characterizes the fifth core. This layer is a bit dryer and seems to be more compact. Besides that, the core is uniform with light lamination and a few darker spots.

The sixth core is generally uniform with a crushed shell at 425 cm and lighter brown area from 431 to 438 cm. In addition, there is authigenic carbonate at 450 and 470 cm.

In the seventh core a large part from 550 to 588 cm missing. Otherwise, the core is uniform with a transition from a light to slightly darker grey colour in the bottom at around 600 cm.

Core number 8 also has lot of missing material. The sediment can be described as uniform laminated, also spotted and contains lenses made out of silt.

The last core is relatively uniform except lighter grey lenses with brown pieces in it at 750 and 765 cm. At the bottom of this core a few parts are missing.

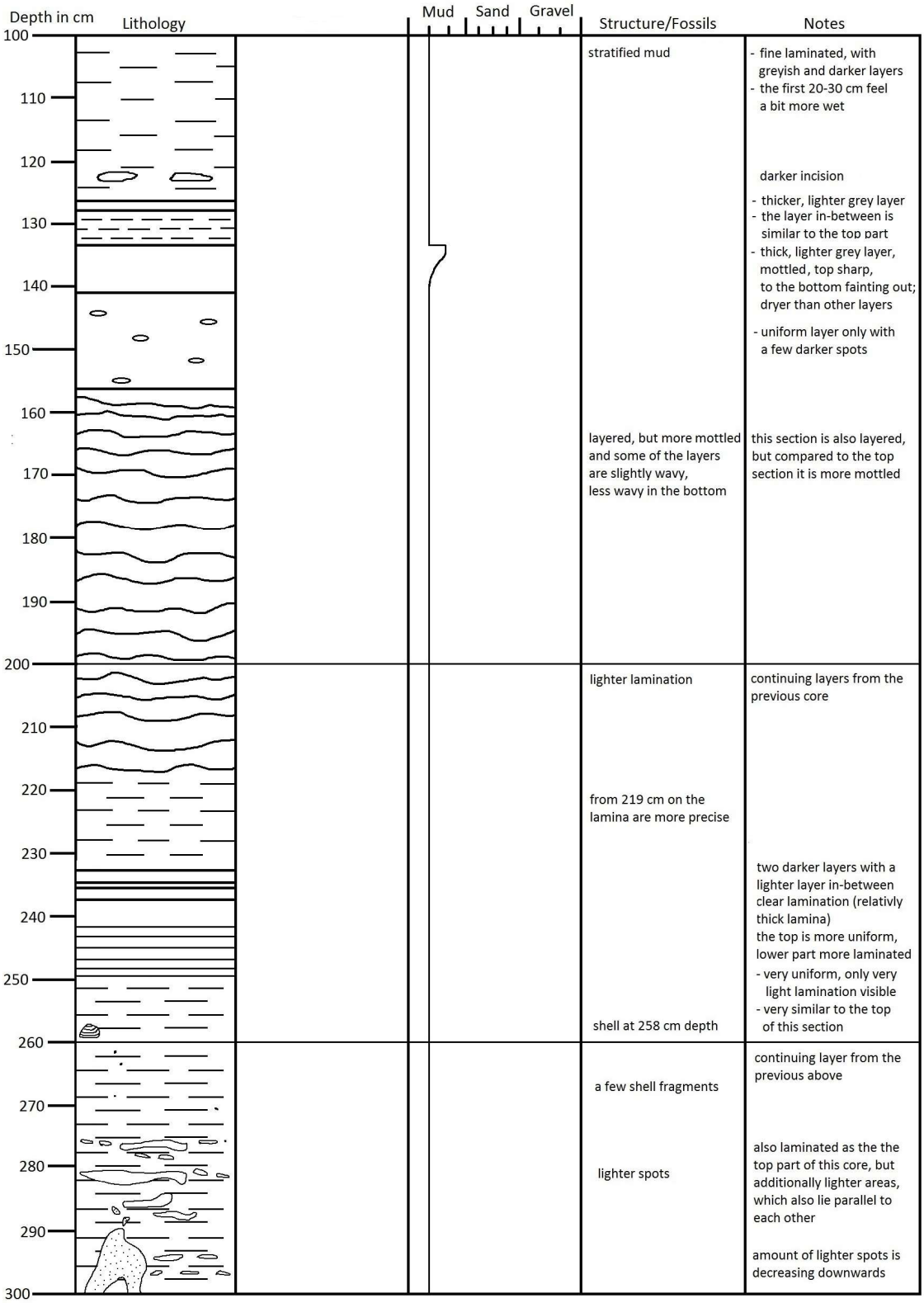
Depth in cm
Lithology
Mud
Sand
Gravel
Structure/Fossils
Notes
100
110
120
130
140
150
160
170
180
190
200
210
220
230
240
250
260
270
280
290
300
stratified mud
- fine laminated, with greyish and darker layers
- the first 20-30 cm feel a bit more wet
darker incision
- thicker, lighter grey layer
- the layer in-between is similar to the top part
- thick, lighter grey layer, mottled, top sharp, to the bottom fainting out; dryer than other layers
- uniform layer only with a few darker spots
layered, but more mottled and some of the layers are slightly wavy, less wavy in the bottom
this section is also layered, but compared to the top section it is more mottled
lighter lamination
continuing layers from the previous core
from 219 cm on the lamina are more precise
two darker layers with a lighter layer in-between
clear lamination (relativly thick lamina)
the top is more uniform, lower part more laminated
- very uniform, only very light lamination visible
- very similar to the top of this section
shell at 258 cm depth
continuing layer from the previous above
a few shell fragments
also laminated as the the top part of this core, but additionally lighter areas, which also lie parallel to each other
lighter spots
amount of lighter spots is decreasing downwards

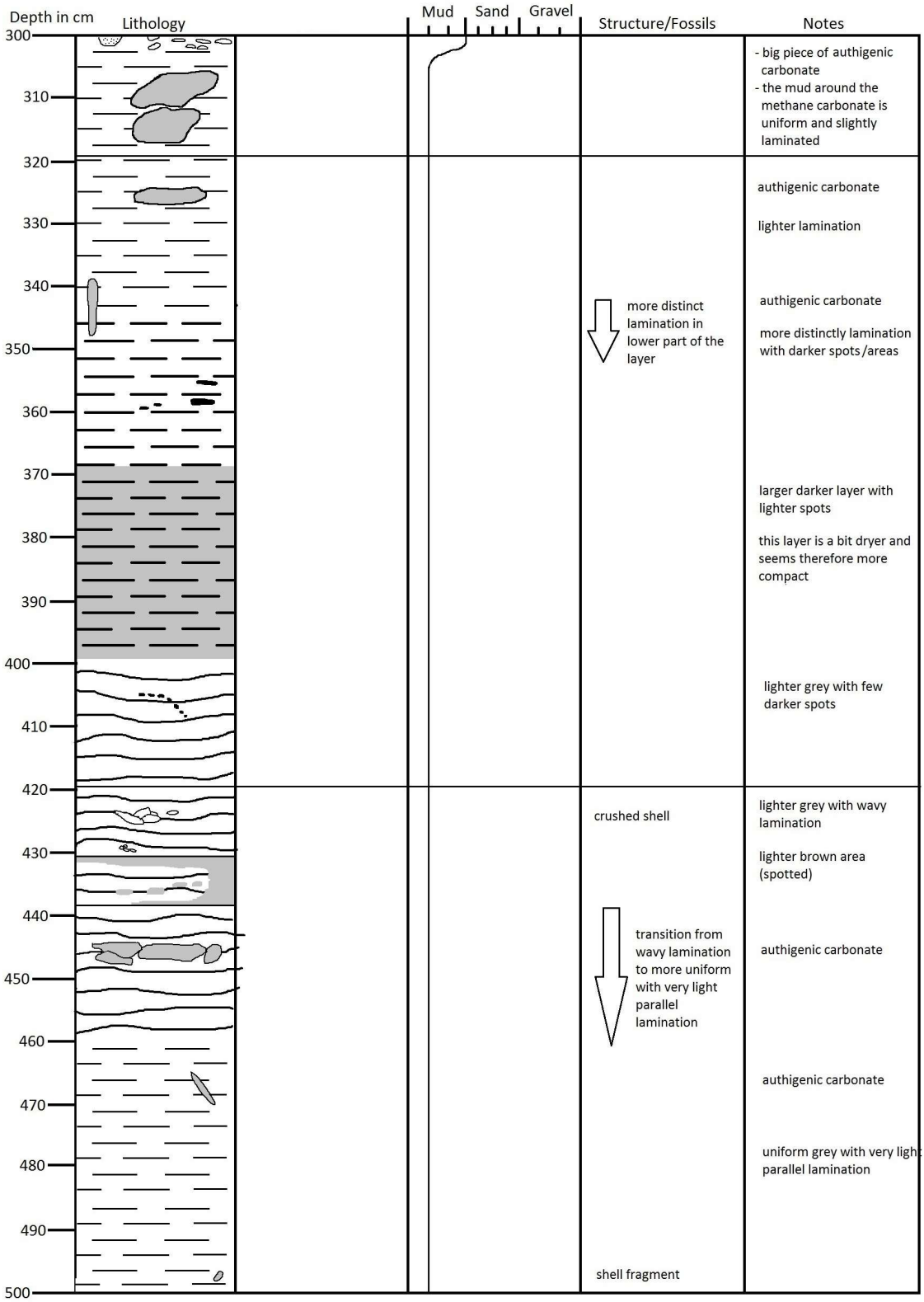
Depth in cm
Lithology
Mud
Sand
Gravel
Structure/Fossils
Notes
300
310
320
330
340
350
360
370
380
390
400
410
420
430
440
450
460
470
480
490
500
- big piece of authigenic carbonate
- the mud around the methane carbonate is uniform and slightly laminated
authigenic carbonate
lighter lamination
authigenic carbonate
more distinct lamination in lower part of the layer
more distinctly lamination with darker spots /areas
larger darker layer with lighter spots
this layer is a bit dryer and seems therefore more compact
lighter grey with few darker spots
crushed shell
lighter grey with wavy lamination
lighter brown area (spotted)
transition from wavy lamination to more uniform with very light parallel lamination
authigenic carbonate
authigenic carbonate
uniform grey with very light parallel lamination
shell fragment

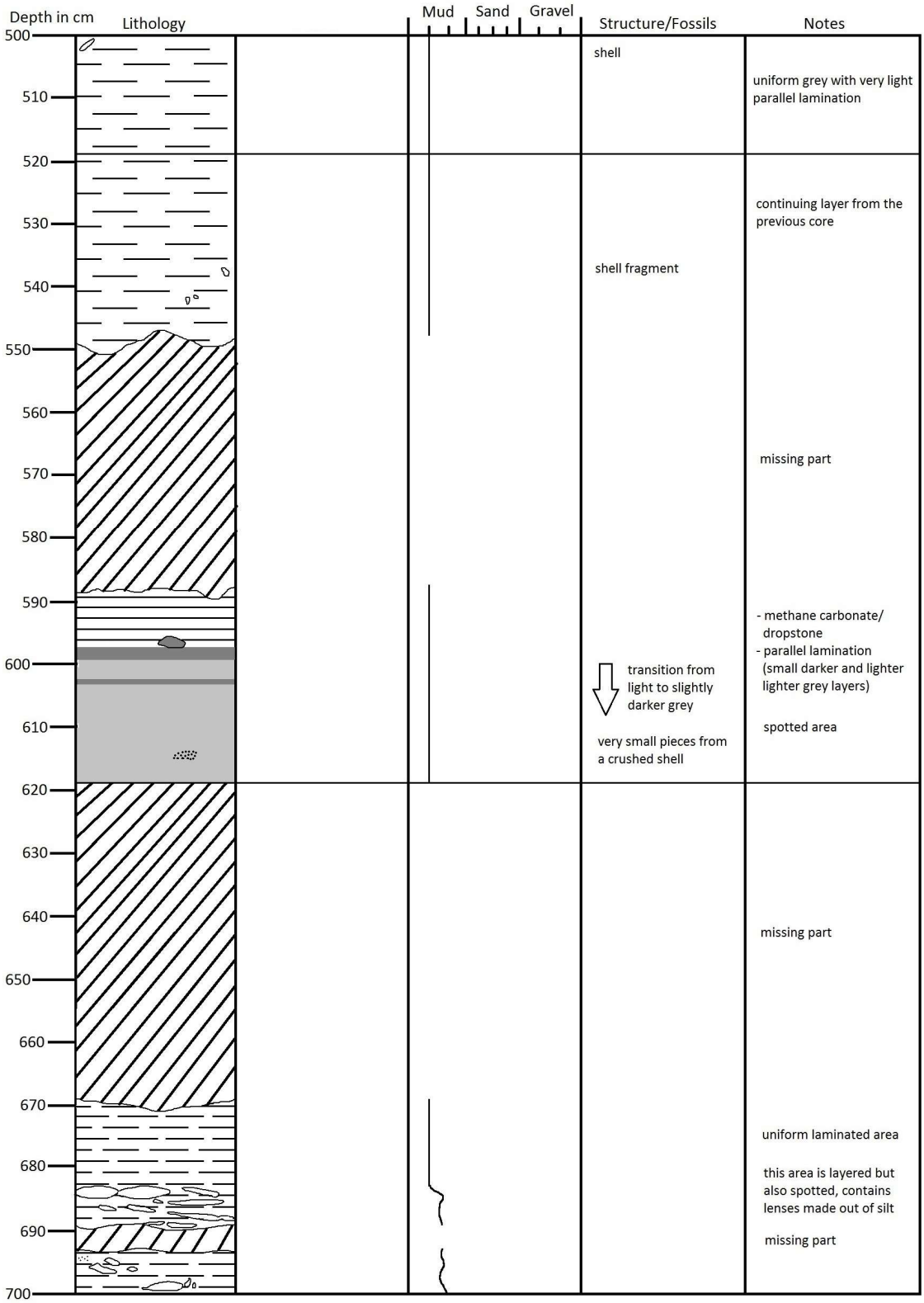
Depth in cm
Lithology
Mud
Sand
Gravel
Structure/Fossils
Notes
500
510
520
530
540
550
560
570
580
590
600
610
620
630
640
650
660
670
680
690
700
shell
uniform grey with very light parallel lamination
continuing layer from the previous core
shell fragment
missing part
- methane carbonate/ dropstone
- parallel lamination (small darker and lighter lighter grey layers)
transition from light to slightly darker grey
spotted area
very small pieces from a crushed shell
missing part
uniform laminated area
this area is layered but also spotted, contains lenses made out of silt
missing part

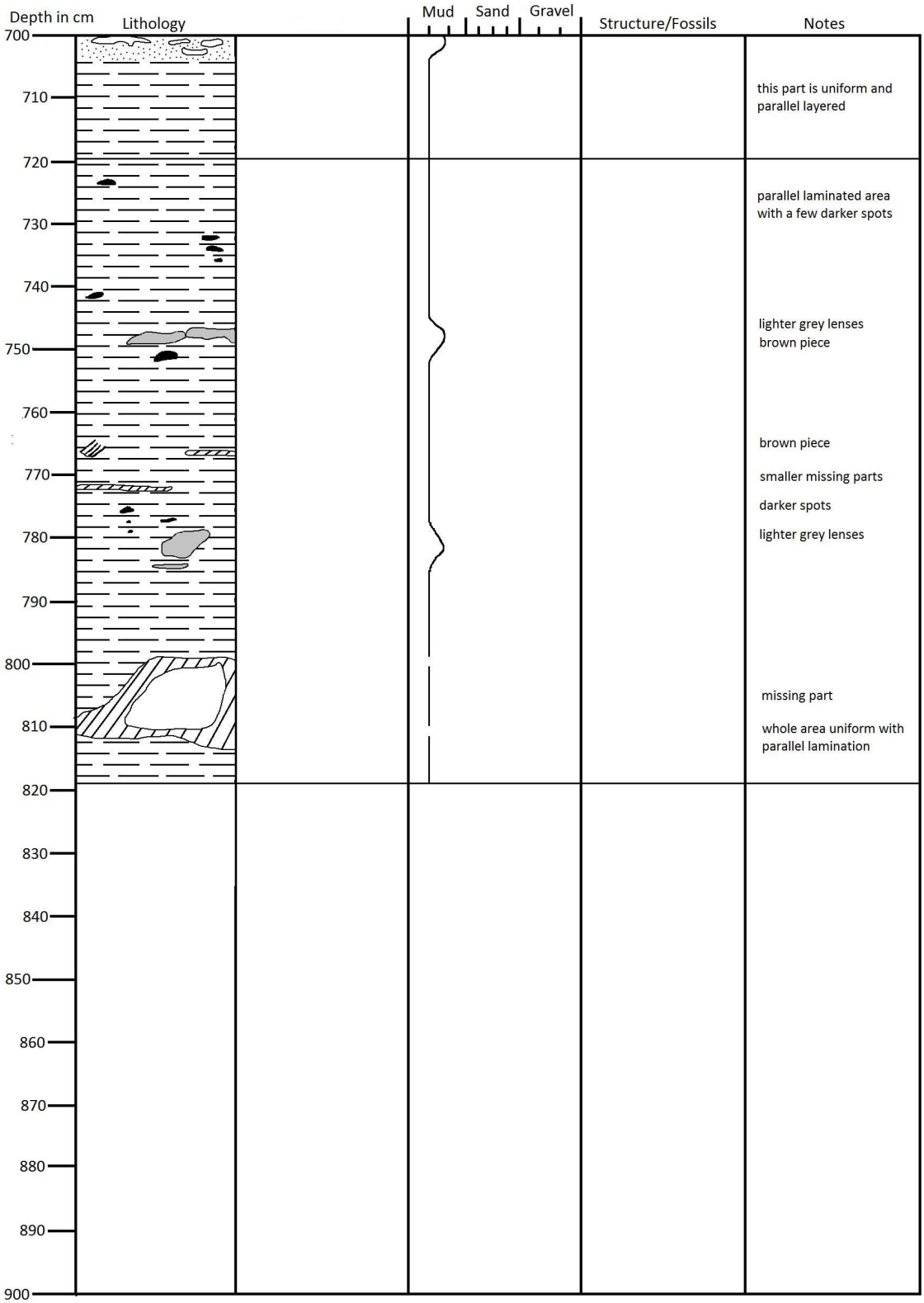

Figure 16: *Core description of the HH15-1255PC core*

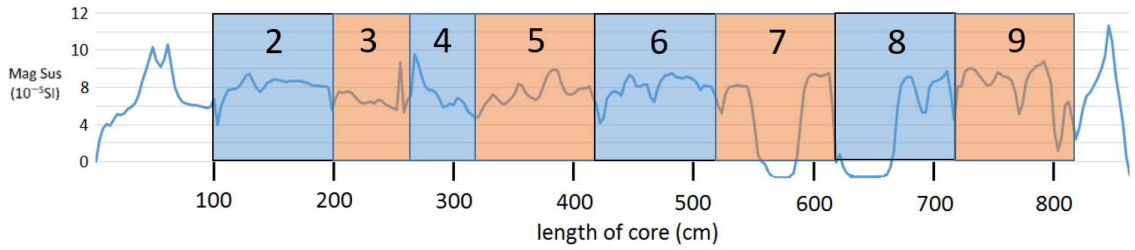

Figure 17: *Diagram showing the onboard logging of magnetic susceptibility with the different core sections*

3.2 X-ray images

With the Geotek x-ray core imaging system it was possible to scan the core. This was done on un-opened core sections.
If one core appears lighter than another, it has nothing to say about the sediment, it is due to the fact that the contrast was adjusted in a way to make it possible to see the structures.
The marks on the size show the length of the cores measured in cm.
The x-ray images were taken before the cores were opened and it was the first time to see the inside of the core.

With the x-ray images (Fig. 18), it is possible to see changes in the sediment along the core. Different grain sizes, density and type of sediment will give different shades of grey on the images. In addition, clasts and shells can be made visible.
Many different layers throughout the whole core characterize the second fraction with one distinct darker layer at around 135 cm. This layer has a relatively sharp top and is fading out towards the bottom.
In section 3 a few layers can be seen in the upper part of the core until around 215 cm. After that, the core is more uniform. There are also a few rocks visible at 225 and 240 cm, which are identified as autigenic carbonate. Section number 4 is uniform with rocks in the lower part.
The fifth section is very uniform with the exception of containing a large and darker layer from 371 to 382 cm. Like the darker layer in section 2, this layer also has a sharper boundary in the top and fading out towards the bottom.
The sixth section has an accumulation of rocks from 441 to 453 cm. Generally speaking, the core is uniform without any layers.

In section 7, 8 and 9 large parts of the core are empty. There is one carbonate rock at 545 cm, but other than that do the cores not show any distinct features.

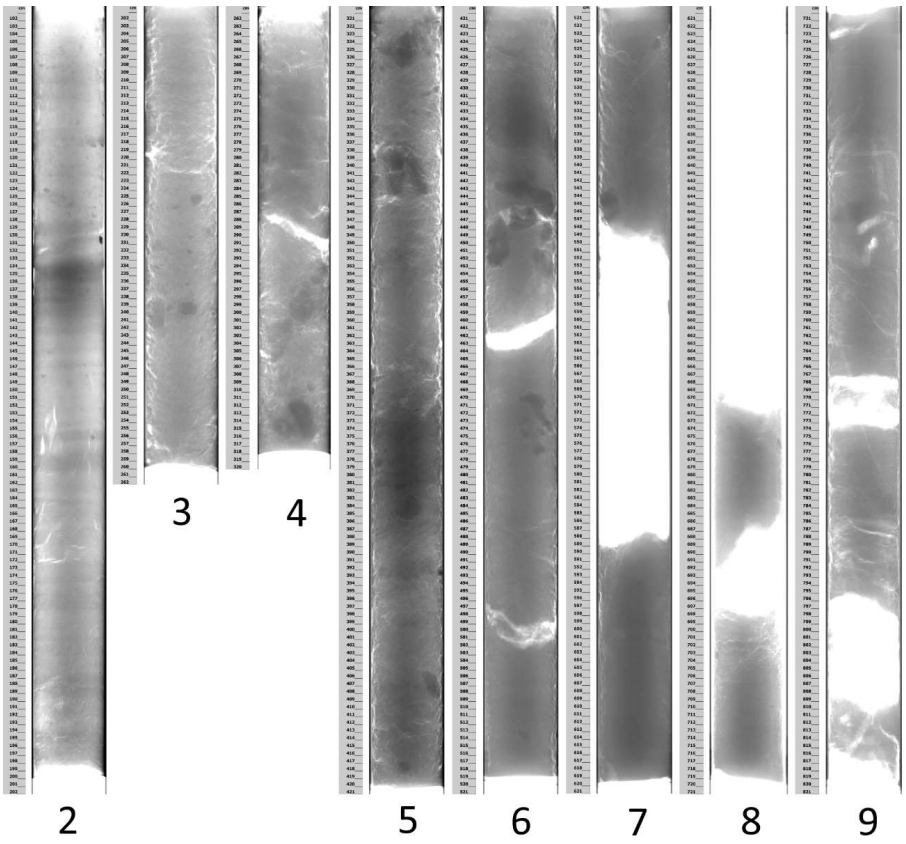

Figure 18: *X-ray images of the different sections. The marks on the side show the cores measured in cm. To see the inner structures as good as possible, the contrast of the images has been adjusted. This leads to that some core sections appear darker.*

3.3 Water content and magnetic susceptibility

The magnetic susceptibility measurements (Fig. 19) were done by a Multi-Sensor-Core logger with a resolution of 1 cm.
The magnetic susceptibility is measured proportionally and indicates to which degree the sediment was magnetized.

The curve for the magnetic susceptibility measurements shows high variability. Most of the values are lying between 10 and 15.
In those parts, where the values are around zero, there was no material in the core.
There are no distinct peaks where the values are completely higher than usual.
Generally said, the values are a bit higher in the upper part of the core.

The water content curve (Fig. 19) shows large variations along the core. The values, measured in percentages, are varying between 20 and 35 %.
Especially in the upper 50 cm, from 300 to 450 cm the content varies. At about 370 and 430 cm there are two troughs in the curve with lower water content.
From 450 cm on, the curve still shows up and downs but not as distinct as before.

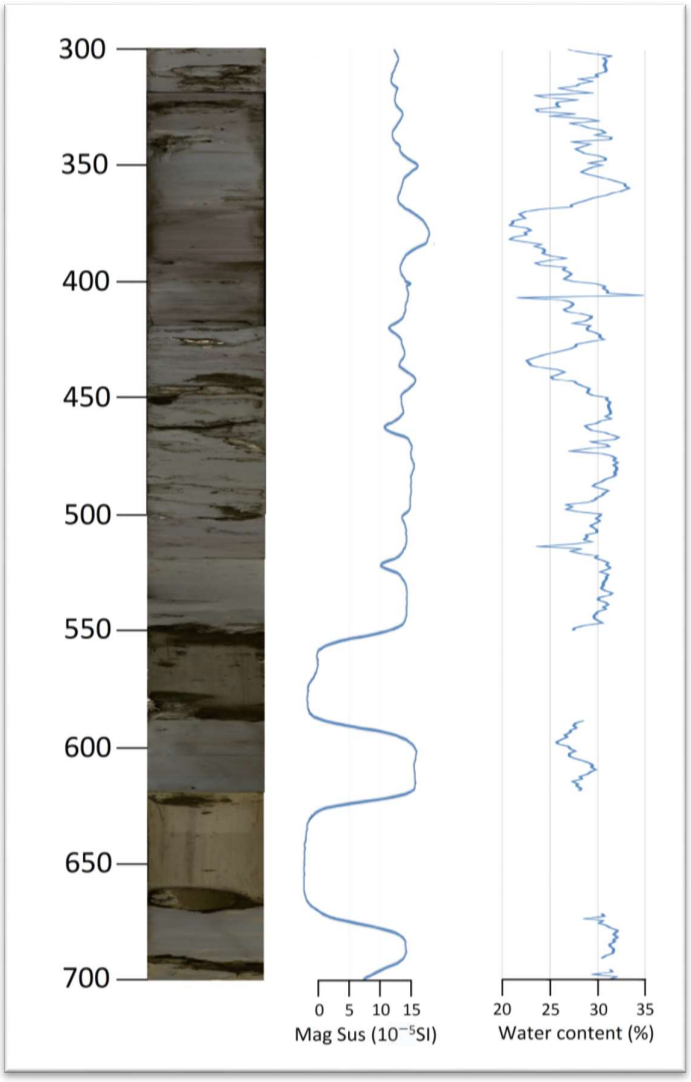

Figure 19: *Magnetic Susceptibility and water content plotted along the core*

3.4 Foraminifera analysis

A large amount of foraminifera has been collected to be able to make profound statements about their distribution. The part of the core where the foraminifera analysis was done is from 300 to 700 cm.

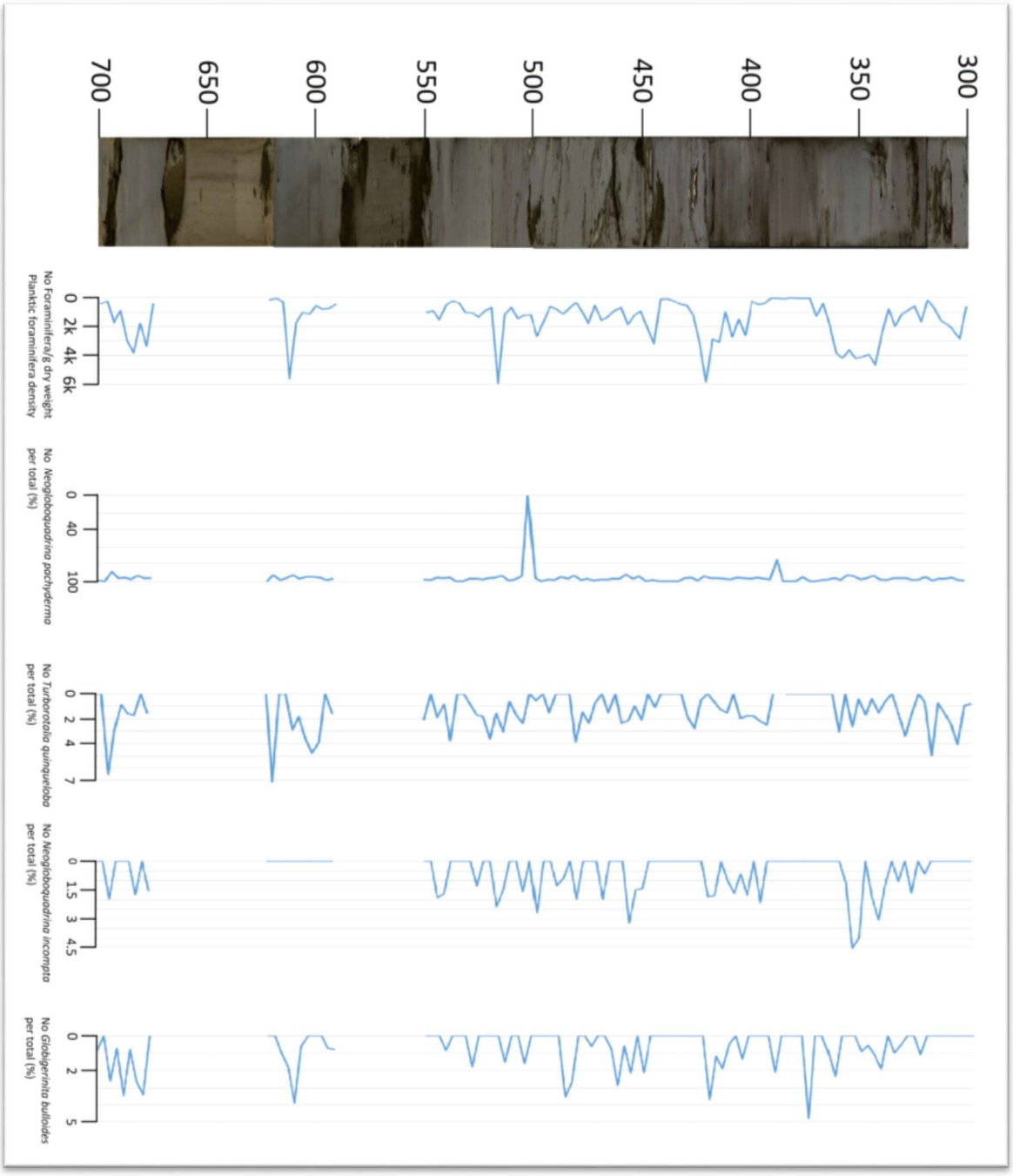

Figure 20: *Distribution of the most abundant planktic foraminifera plotted along the core*

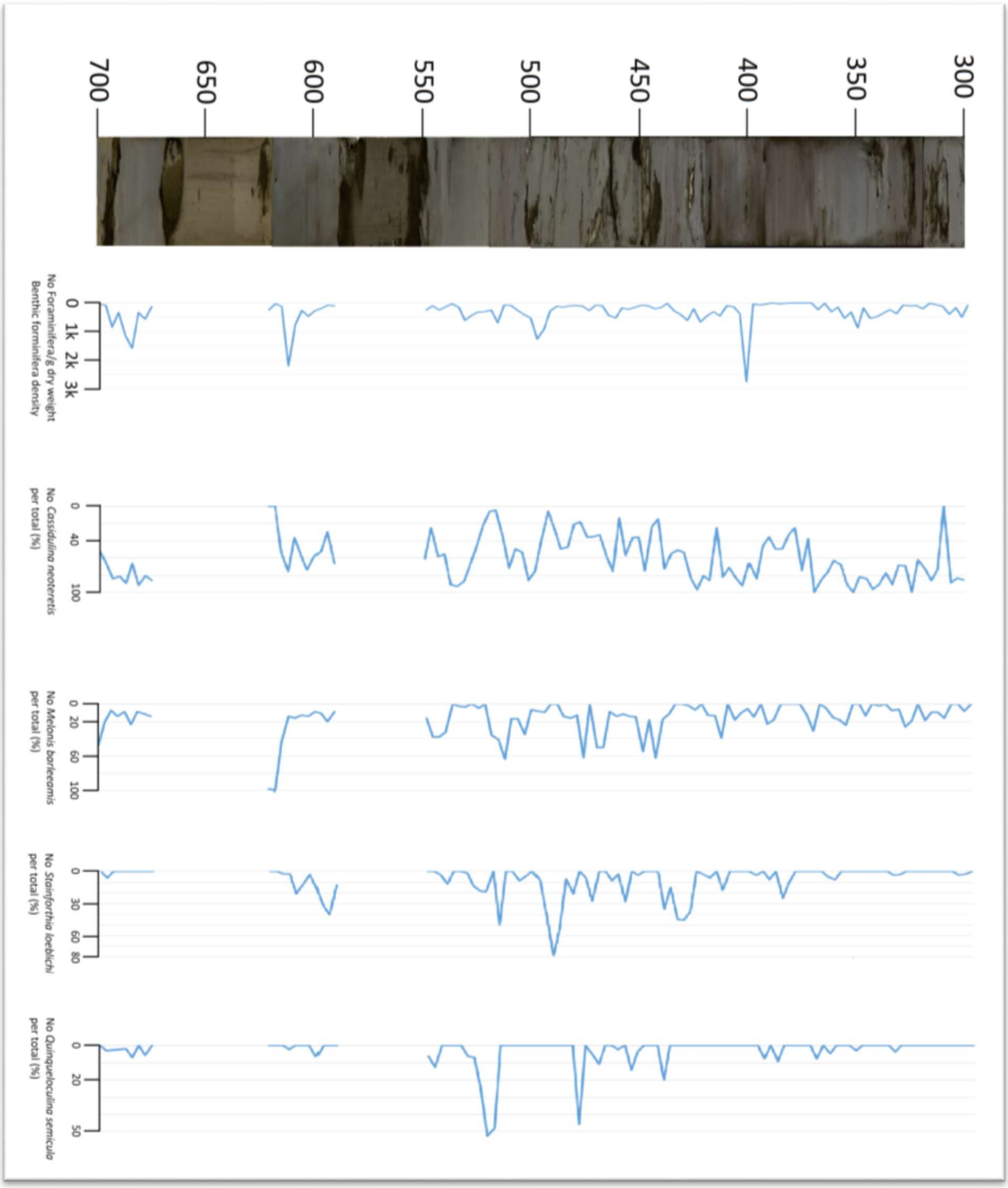

Figure 21: *Distribution of the most abundant benthic foraminifera plotted along the core*

3.4.1 Foraminifera density

The density curve is presented as the depth of the core in cm is plotted against the amount of foraminifera per gram dry weight on the y-axis. This curve gives a general overview about the amount of foraminifera along the core.

The first 36 cm of the distribution curve for planktic foraminifera (Fig. 20) show an average amount of foraminifera. After that from 336 to 363 cm, there is a large amount of foraminifera with a density of around 4,000 no/gdwt followed by a part with barely any foraminifera from 363 to 399 cm. In the next 20 cm, there is another peak where the maximum density reaches up to almost 6,000 no/gdwt. At 435 cm, a minimum with only few foraminifera is located, but not as big as the minimum from 363 to 399 cm. After that from 440 cm onwards, the density is generally varying between 200 and 3,200 no/gdwt. In that section there are two peaks with 5,953 and 5,600 no/gdwt and also a minimum with only 60 no/gdwt at 614 cm.

The calculated density curve of benthic foraminifera (Fig. 21) shows similar pattern as the curve for planktic foraminifera, even though the density of benthic species is lower than for the planktic. Here the no/gdwt is generally varying between 200 to 1,000.

As for the benthic foraminifera curve an increased amount of foraminifera can be found in the area around 350 cm followed by an absence of foraminifera, which is located between 372 and 399 cm.

After that, the curves are quite alike, showing peaks at the same depth. For example at 608 cm for both plantic and benthic foraminifera, a peak with 2,200 forams/gdwt is followed by an area with a low density.

3.4.2 Foraminifera species analysis

The cold-water species *Neogloboquadrina pachyderma* is the overall dominant species. In some samples up to 2,000 individuals can be found. Since the amount of *N. pachyderma* is very large, the graph does not show many variations. In most of the samples, the amount of *N. pachyderma* is around 95 % of all planktic species. Only at 387 and 501 cm the graph has lower values.

The curves for *Turborotalia quinqueloba*, *Neogloboquadrina incompta* and *Globigerinita bulloides* follow a similar pattern with some variations. It also needs to be considered, that besides *Neogloboquadrina pachyderma,* all other planktic foraminifera species only appear in smaller numbers. Small changes in the amount can have a high influence on the shape of the curve. That is also the reason why the curve is showing so many fluctuations.

For benthic foraminifera, the species analysis has been done in a same way as for the planktic foraminifera. The by far most abundant benthic species is *Cassidulina neoteretis*. The distribution of benthic species has been illustrated in figure 21.
There is an increased amount of *Cassidulina neoteretis* from around 325 to 360 cm, 390 to 420 cm and two peaks at 501 and 534 cm. The curve shows in general a higher amount of *Cassidulina neoteretis* in the first half of the curve.
In comparison to that, the other benthic foraminifera *Melonis barleeanis*, *Stainforthia loeblichi* and *Quinqueloculina semicula* show an increase in the second half. Only some of the peaks are aligning. Most of the times, the curves show peaks at different locations.

3.5 Dating Results

The results of the radiocarbon dating (Table 1) from the ^{14}CHRONO Centre in Belfast, Ireland give ^{14}C ages for the different samples (Fig. 22) with an uncertainty of a few hundred years. The youngest sample has a calendric age of 20,984 years and the oldest sample is 32,356 years old (Table 2). The age difference between the oldest and the youngest sediment is around 10,000 years.

It is also important to notice that there is an age reversal. The sample at 333 cm is older than the one below at 351 cm.

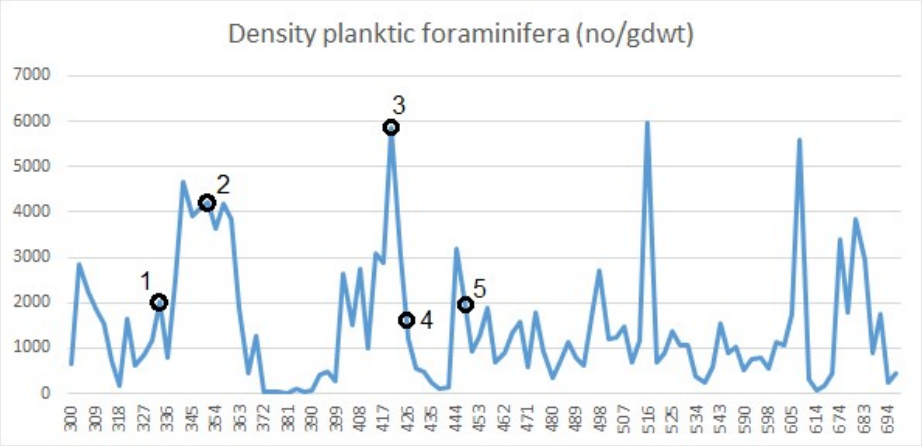

Figure 22: *Density curve of planktic foraminifera. The samples, which were used for radiocarbon, dating were taken from the marked position on the curve.*

The results of the radiocarbon dating (Table 1) from the ^{14}CHRONO Centre in Belfast, Ireland give ^{14}C ages for the different samples (Fig. 22) with an uncertainty of a few hundred years. The youngest sample has a calendric age of 20,984 years and the oldest sample is 32,356 years old (Table 2). The age difference between the oldest and the youngest sediment is around 10,000 years.

It is also important to notice that there is an age reversal. The sample at 333 cm is older than the one below at 351 cm.

Table 1: *Lab results from the ^{14}CHRONO Centre in Belfast, Ireland showing the depth of the sample and their ^{14}C ages*

UBANo	Sample ID	Material Type	^{14}C Age	±
UBA-36747	HH15-1255PC, 420cm	Foraminifera	26519	151
UBA-36748	HH15-1255PC, 447 cm	Foraminifera	30506	229
UBA-36749	HH15-1255PC, 351 cm	Foraminifera	19568	82
UBA-36750	HH15-1255PC, 333 cm	Foraminifera	23113	110
UBA-36751	HH15-1255PC, 425 cm	Bivalve	29681	207

Table 2: *Calculated calendric ages*

sample nr.	sample name	14C age	±	14C ages - reservoir age	**Calendric Age calBC**	±
Sample 1	HH15-1255PC, 333 cm	23113	110	22673	**25433**	**387**
Sample 2	HH15-1255PC, 351 cm	19568	82	19128	**20984**	**291**
Sample 3	HH15-1255PC, 420cm	26519	151	26079	**29060**	**343**
Sample 4	HH15-1255PC, 425 cm	29681	207	29241	**31721**	**328**
Sample 5	HH15-1255PC, 447 cm	30506	229	30066	**32356**	**185**

3.6 Isotope Measurements

The results for $\delta^{13}C$ for planktic foraminifera are varying between -1 and -7 ‰ deviation from the standard. In the diagram (Fig. 23), the upper parts of the curve with higher values are in general flatter, whereas the lower parts of the curve are sharp. The four points on the curve with low values are at 318, 462, 516 and 683 cm.
The $\delta^{18}C$ values for benthic foraminifera are varying between -1 and -11 ‰. The curve is also characterized by many variations. At 318 and 677 cm the measurements reach low values. Between 408 and 480 cm the distance between peaks is smaller.

The $\delta^{18}O$ values for plankic foraminifera are very stable at 5 ‰. Towards lower parts of the core, the values are slightly decreasing towards 4 ‰ without reaching this value.
The same applies for the results for the $\delta^{18}O$ values from benthic foraminifera. The curve is also stable, but here the values are lying a bit higher between 5 and 6 ‰.

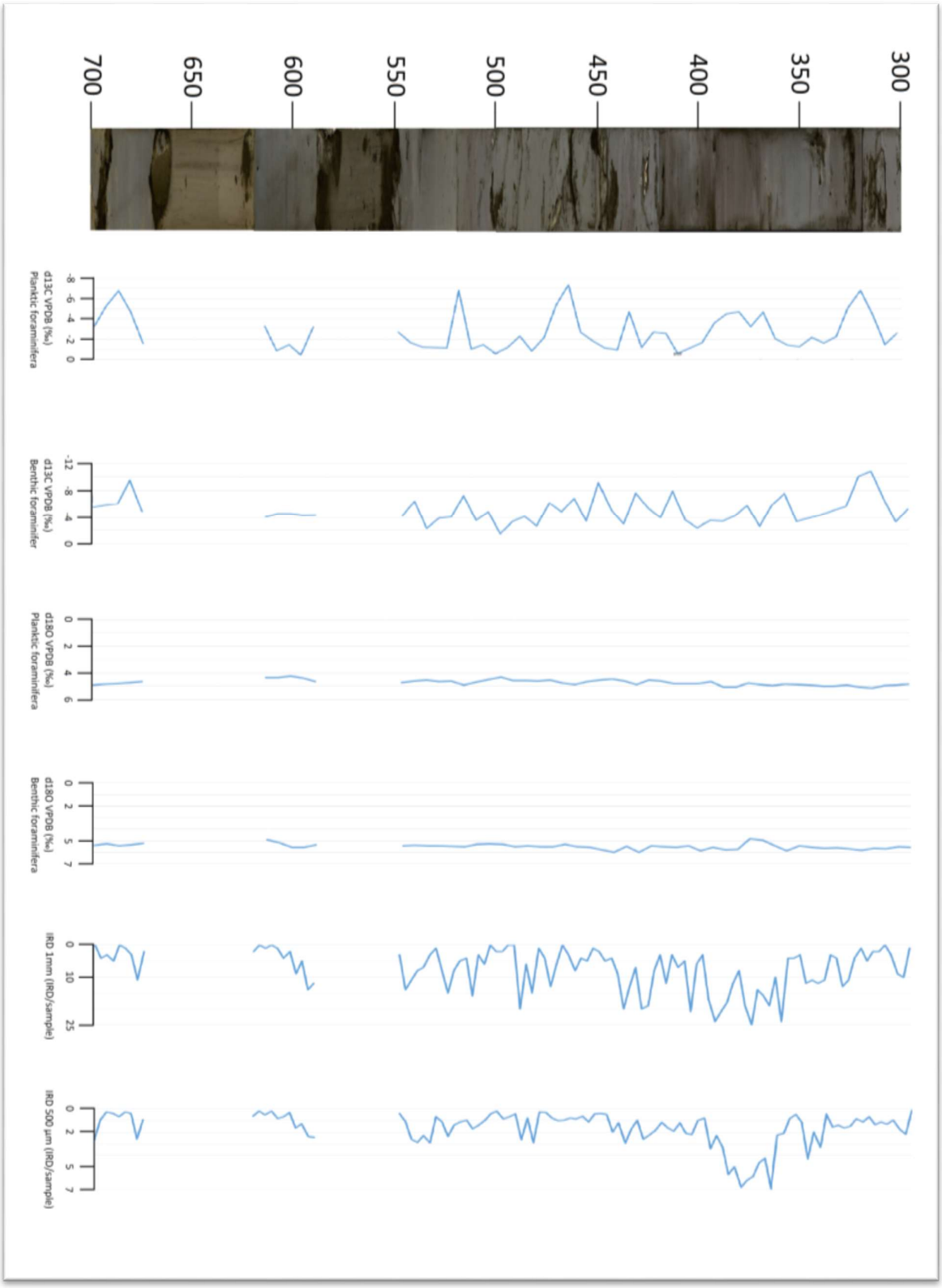

Figure 23: *Carbon/Oxygen isotope measurements from both planktic and benthic foraminifera and IRD plotted along the core*

3.7 IRD analysis

The IRD analysis (Fig. 23) has been done in the 1 mm and 500 µm fraction from 300 to 697 cm.
Both curves follow a similar pattern. From 300 cm on the amount of IRD is generally increasing and reaching a peak at around 370 cm. After that the IRD is decreasing.

The samples for the 1 mm fraction contain an amount of IRD from 0 to 25. The curve reaches its highest value at 378 cm. But even after that, quite many samples have a higher amount of IRD. The amount of IRD though is fluctuating a lot along the curve, especially with samples that are right next to each other. One sample can have 20 IRD, the following one almost none and then going up to a high amount again.
The curve for the 500 µm fraction shows less fluctuations than the 1 mm curve. A large amount of IRD is found from 369 to 390 cm. Here the amount IRD reaches almost 140. This area can also be seen as a distinct peak along the curve. Not clear visible peaks, but a bit larger amount of IRD compared to the curve are located at 441, 486 and 534 cm.

4 Age model

Before the results can be correlated with events, an age model needs (Fig. 24) to be constructed. This age model shows in which timeframe the core is located and makes it possible to link the data with similar results from previous works.

The results for the ^{14}C measurements on the HH-1255PC core show an age reversal, where one samples is older than the other but at the same time lying above in the core.
There are a few explanations for that. In tectonic areas, where the sediment can get deformed, older sediment can lie on top of younger ones. But since the core is from the ocean floor this is most likely not the case. Another factor is the contamination of the samples. The core has been taken from a methane seep. The carbon, which is released from the seeps, can form coatings around the foraminifera. This can lead to different ages (Lembke et al., 2003). Another explanation for the age reversal can be due to mistakes in the lab. The samples could be labelled incorrectly. Mistakes could have also been made when the ^{14}C was measured in the lab in Ireland.

Another event, which can be included in the age model, is a coarse layer from 370 to 400 cm. Along this section of the core, the sediment shows a red-brown colour and a larger grain size. As well, the different measurements like the magnetic susceptibility and water content show clearly visible changes at this part of the core. However, foraminifera are missing in this layers, neither planktic, nor benthic species are found.
As described by Rasmussen et al. (2006), the coarse layer can be correlated with a debris flow event, which has been dated to be 23,440 ± 315 cal years old (Elverhøi et al., 1995). This event can be added to the age model as being another component to get more accuracy.
For creating the age model, the results of ^{14}C measurements were used. They give a precise depth, but some uncertainties about the age. Sample 1 was not used in the age model since it gave an older age than sample 2 and did not fit in along the connected line between the samples.

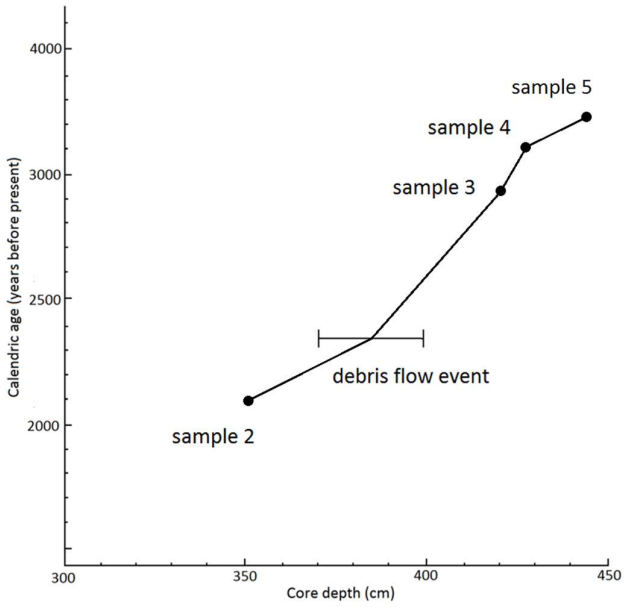

Figure 24: *Age-model showing the calibrated radiocarbon age plotted against the depth. The debris flow event, which is illustrated as a bar, covers a larger part of the core.*

The age model shows the range for the calendric age in comparison with the depth of the core. It is possible to see the general trend of how the age differs along the core. Since the sedimentation rate (Table 3) differs quite a lot between the samples, it is not possible to reconstruct an age model for the whole core just from those four dating results. The calendric age of other parts from the core can just be estimated.

However, the age model gives valuable results for a period between 2,000 and 3,000 years before present.

Table 3: *Sedimentation rates between the dated samples*

Measurements between samples	distance between depths	difference between Calendric Ages	sedimentation rate - cm/kyears
Sample 2/3	69	8076	8.54
Sample 3/4	5	2661	1.88
Sample 4/5	33	635	34.65

5 Discussion

In this chapter, the results will be interpreted and put in relation with literature. The goal of this work is to reconstruct the climate conditions at the end of the last glaciation and during the last glacial maximum by correlating the data from the core HH15-1255PC with different climatic periods and events.

The main focus will be put on the correlation of the graphs with Dansgaard-Oeschger and Heinrich events. For comparison, previous studies will be used, which were done in the Fram Strait and on ice cores from the Greenland ice sheet.

5.1 Correlating magnetic susceptibility

Four AMS ^{14}C dates in combination with age of well-known lithological events provide the time frame and the basis for the age model. About 12,000 years are lying between the oldest and the youngest dated samples. In the core, this age covers a depth of 96 cm. By expecting a similar sedimentation between the dated samples, it is possible to estimate the age of the sediment above and below the dated samples. For a more accurate correlation, the magnetic susceptibility curve of the core was compared with magnetic susceptibility measurements from the core JM03-373PC2, which has been analyzed and dated by Jessen et al. 2010. Both curves follow a similar pattern and by aligning the peaks, the results can be correlated (Fig. 23).

The youngest sediment in the HH15-1255PC core at 100 cm depth can be expected to be around 10,000 years old. At 300 cm where the foraminifera samples were taken, the age is about 19,000 years.

In both cores, mass transport deposits from a debris flow event are found (Jessen et al., 2010) (Fig. 24). In the JM03-373PC2 core though, those deposits are much thicker than in the HH15-1255PC core.

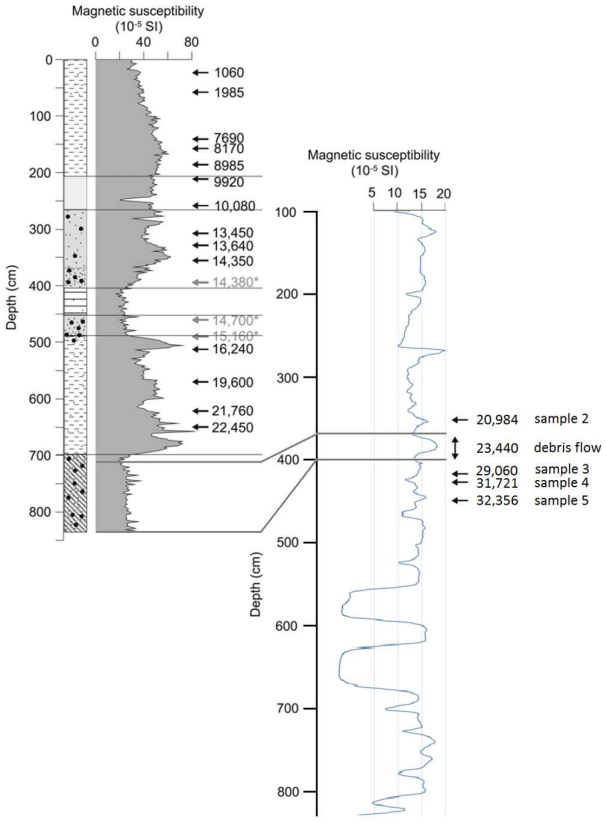

Figure 25: *Modified figure from Jessen et al. 2010 comparing the magnetic susceptibility measurements from both cores HH15-1255PC and JM03-373PC2*

5.2 Correlating data with Greenland ice core

For the identification of certain events, the core needs to be correlated with curves from previous studies.

The ice core from the Greenland Ice Sheet Project Two (GISP2) (Fig. 26) provides data with high resolution, which can be compared with results from the HH15-1255PC core. The GISP2 core was drilled in the middle of the Greenland Ice and has a total length of 3,053 m (Andersen, 2004).

Figure 26: *Location of the Greenland Ice Sheet Project Two (researchgate.net, 2018. Researchgate)*

Figure 27 shows the $\delta^{18}O$ measurements of the Greenland ice core. The ratio of ^{18}O and ^{16}O is depending on temperature and ice volume. This can be directly linked to the climate. Higher $\delta^{18}O$ values indicate a warmer climate, whereas lower $\delta^{18}O$ values mean colder conditions.
For comparison, the graph for the density of planktic foraminifera is used. This graph does not represent temperature, but rather how stable the conditions are. The end of the last glacial period is characterized by Dansgaard-Oeschger events. Those periods show climate cycles with rapid warming followed by a gradual cooling (Cacho et al., 1999).
It has been suggested that during a fast warming large amount of the ice sheets break apart. During those periods also Heinrich events take place (Alvarez-Solas et al., 2010). A large amount of IRD is transported by icebergs and deposited on the seafloor. Meltwater supply from icebergs can result in weakening the ocean circulation (Rahmstorf, 2002).
Foraminifera prefer clear waters with less disturbance and stable conditions over a certain period of time. This is not the case during Heinrich events and the density of planktic foraminifera is much lower.
During periods with a slow cooling, also called stadials, the conditions are more stable and foraminifera appear in a higher density. In addition, most of the foraminifera species that are found in the HH15-1255PC core are Arctic species and will appear with a higher number during colder periods. That is also another reason why the foraminiferal density is higher during stadials.
The curve for the density of planktic foraminifera is not following the $\delta^{18}O$ curve identically, but shows the same fluctuations during stadials and interstadials. Therefore, the curves can be used for correlation and to find out at which depth Dansgard-Oeschger and Heinrich events can be seen in the HH15-1255PC core.

First of all the results from the carbon dating have been used to set the 20,000 and 30,000-year mark in the graph. The youngest dating result gives an age of 19,568 years and the oldest one 30,506 years. Of course, there are some uncertainties with the accuracy of the dating results within a few hundred years. Still it is possible to correlate the Dansgaard-Oeschger events from the HH15-1255PC core with the Greenland Ice core, since the Dansgaard-Oeschger events last over a longer period (few thousand years) compared to the inaccuracy of the dating results with only a few hundred years.
Between 20,000 and 30,000 years, the curve for the foraminiferal density shows clear fluctuations, which correspond to the $\delta^{18}O$ measurements of the Greenland ice core. By comparing the two curves with each other, Dansgaard-Oeschger event 2, 3 and 4 can be

correlated in that time frame. Further down in the core, the peaks of the curves can be correlated with Dansgaard-Oeschger event 5 to 11. Since the age of these events are know, it is now possible to set more date marks on the core. This shows that the sedimentation rate at deeper parts of the core is similar to the one between 20,000 and 30,000 years.

To correlate Heinrich events, the curves for the detrital carbonate of the Deep Sea Drilling Project has been compared with the 500 μm IRD fraction of the HH-1255PC core, seen in figure 27. Detrital carbonate originates from the erosion of carbonate rock and like IRD shows the amount of sediment depositions in the oceans. The IRD was counted both in the 500 μm and 1 mm fraction of the core. The 500 μm curve though shows less fluctuation between different samples and a clearer signal of the Heinrich events along the core. That is why the 500 μm fraction was chosen for correlation. First of all the 20,000 and 30,000 year marks were put in the IRD curve. The same marks were used as for the Dansgaaed-Oeschger event correlation. Except that the peaks are not that sharp, the IRD curve follows the same pattern as the detrital carbonate curve from the IODP core.

From 370 to 400 cm the core contains a high amount of larger grain material, which derives from a debris flow (Jessen et al., 2010). In the same timeframe as the debris flow occurs, also Heinrich event 2 takes place. The signal at is this position of the core is a combination of both the debris flow and Heinrich event 2.

Heinrich event 2 is correlated at around 24,000 years before present with a strong signal. Whereas Heinrich event 3 shows a weaker but still clearly visible signal at around 29,000 years. Both Heinrich event 2 and 3 lie in the time frame where the dating results were done, so therefore they are well constrained by dates and correlations.

The next distinct peak in the IRD graph appears at around 40,000 years. That is around the same area where Heinrich event 4 happened. The signal though is not that strong as in the IODP core.

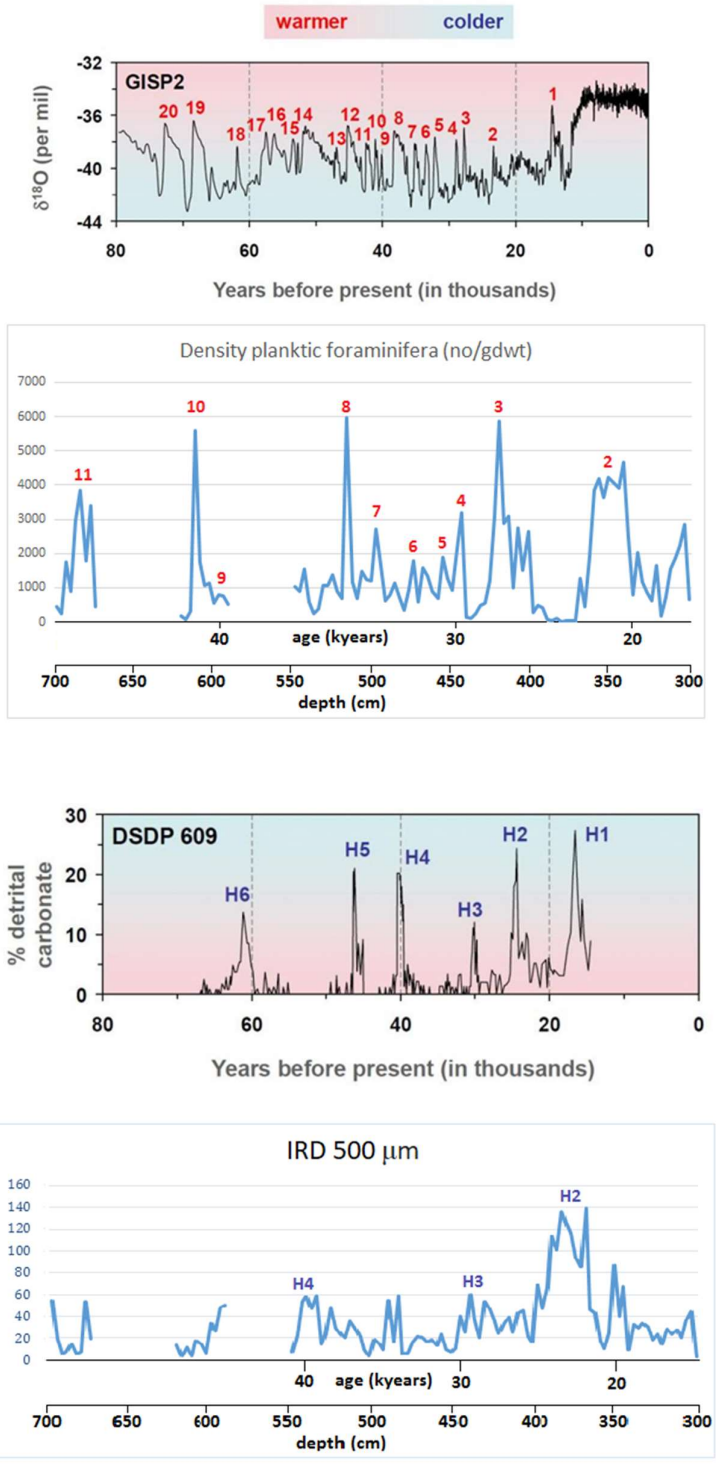

Figure 27: *Comparing the density curve of planktic foraminifera with $\delta^{18}O$ values from the Greenland ice core to correlated Dansgaard-Oeschger events. As well, the 500 μm fraction of IRD is compared with detrital carbonate to identity Heinrich events in the HH15-1255PC core. (ncdc.noaa,gov, 2018. Heinrich and Dansgaard-Oeschger Events)*

In figure 28, the density of both planktic and benthic foraminifera, magnetic susceptibility, water content, IRD (500 μm) and the carbon isotope measurements from benthic and planktic foraminifera have been plotted along the core. During Dansgaard-Oeschger events and Heinrich events these curves show distinct changes depending on the type of event.

Dansgaard-Oeschger events lead to an increase in the density of planktic and benthic foraminifera. These events are characterized by rapid warming followed by a slow cooling. During the cooling phase the conditions are relatively stable and foraminifera population are increasing. (Andersen et al., 2004).

During Heinrich events, the foraminifera density is decreased to a minimum. The influx of Ice Rafted

Debris in the ocean and spread of meltwater lead to low-salinity turbulent conditions and foraminifera cannot flourish.

The magnetic susceptibility does not show any distinct chances during Dansgaard-Oeschger events. Due to the coarse grained material, which was deposed at Heinrich events, the magnetic susceptibility is increased in those periods.

The curve for water content shows high values during Dansgaard-Oeschger and low values during Heinrich events. Since the water holding capacity is highly depending on the grain size, the coarser IRD cannot store as much water as the fine material, which is deposited at Dansgaard-Oeschger events (Wang and Sassa, 2002).

During Heinrich event the amount of IRD is increased (figure 28). It is also possible to see the coarse-grained material, which was deposited through a debris flow during Heinrich event 2 (Jessen et al., 2010).

The $^{13}C/^{12}C$-ratio shows how much dissolved inorganic carbon is available in the ocean and gives a signal of the bio production (Spero et al., 1997). During Dansgaard-Oeschger events, the $^{13}C/^{12}C$ is increased and conditions are in favor for foraminiferal production. That is why the isotope curve for carbon is following a similar pattern as the curve for foraminiferal density.

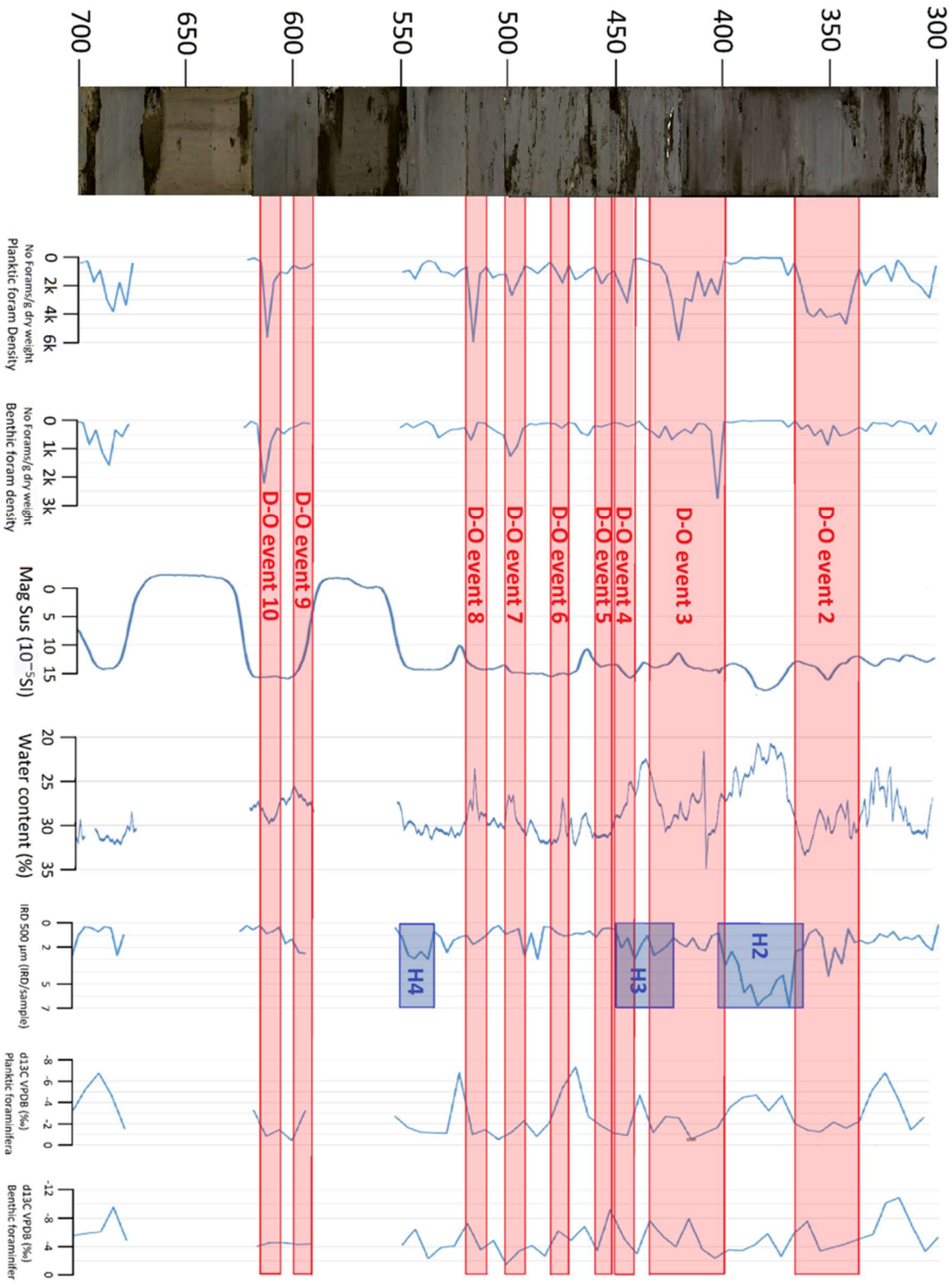

Figure 28: *Foraminiferal density, magnetic susceptibility, water content, IRD and isotope measurements plotted along the core. Dansgard-Oeschger events (red) and Heinrich-events (blue) are highlighted.*

5.3 Foraminifera

Figure 29 shows the amount of the planktic and benthic foraminifera species along the core. Since each foraminifera species is reacting different to changes in parameters, it is possible to obtain more detailed information about the paleoenvironment and paleoclimate.

Neogloboquadrina pachyderma is the most abundant species. In most of the samples, *N. pachyderma* makes up more than 95 % of all foraminifera species. Since the amount of *N. pachyderma* is relative stable along the core, it can be said that at this certain location in the Fram Strait cold, polar water has always been very dominant. Also chlorophyll, which is the main food source for *N. pachyderman*, must have always been available (Kohfeld and Fairbanks, 1996).

Neogloboquadrina incompta is found especially in the second half of Dansgaard-Oeschger events during the cooling phase (stadials). Their occurrence at the ending of these events confirms the fact that the influence of subpolar water increases since *N. incompta* is a foaminifera species that is found in this water mass (Darling et al., 2006; Andersen et al., 2004).

Turbototalita quinqueloba is a foraminifera species that indicates Atlantic water (Schäfer et al., 2001). They are like *N. incompta* pesent during stadials. It can be also observed, that this species appears after the first third of Dansgaard-Oeschger event 2 and 3. Their amount is decreasing towards the ending the events. During the interstadials (rapid warming phase), when large amount of ice break off, the conditions in the ocean are too turbulent for these foraminifera. They appear in higher numbers after the interstadials (rapid warming phase) when conditions are stable enough.
Towards the ending of Dansgaard-Oeschger event, temperatures and the influence of warmer Atlantic water are decreasing.
Their presence during the other Dansgaard-Oeschger events indicates occasionally inflow of warmer water.
During Heinrich event 2 and 3, this species cannot be found, whereas *T. qinqueloba* appears at Heinrich event 4. Meltwater water surges, which occur during Heinrich events, are known to have changed the circulation in the North Atlantic deep water (Vidal et al., 1997). The ocean currents must have been different at Heinrich event 4.

Globigerinita bulloides is found in subpolar water and upwelling areas. As described by Falk-Petersen et al. (2013) glaciated shelves and sea ice can influence upwelling. This foraminifera species can be used as an indicator for how strong upwelling occurred. During Dansgaard-Oeschger event 3 it is noticeable, that there is a relatively long period with no *G. bulloides*. This could be correlated with surges of the Svalbard-Barents Sea ice sheet (Van Kreveld et al., 2000).

Cassidulina neoteretis is a benthic species that lives in chilled Atlantic-derived intermediate water (Andrews and Dunhill, 2003). This species is the most abundant benthic species in this core and shows that Atlantic-derived subsurface water has always been the main influence at this coring site.

Melonis barleeanus can be found in sediments with high organic matter level (Elberling et al., 2002). This foraminifer is more frequent during the older Dansgaard-Oeschger events 4 to 8. The organic supply during those events seemed to have been higher.

The curve for *Stainforthia loeblichi* shows similar results as for *Melonis barleeanus* with higher abundance during the older Dansgaard-Oeschger events. *S. loeblichi* indicates polar water and expended sea-ice cover (Knudsen, 1984). That confirms the fact that the Eurasian ice sheets are retreating. Around 60,000 to 50,000 years those ice sheets reach a maximum followed by a slow decay (Svendsen et al., 2004).

Quinqueloculina seminula are found in tidal-dominated environments. Since the location of the coring site is at a water depth of 1,206 m those foraminifera needed to be transported to this location. At two distinct events during Dansgaard-Oeschger event 6 and 8, this species appears in large numbers. An explanation for this could be that they were transported to this location through debris flow or ocean currents.

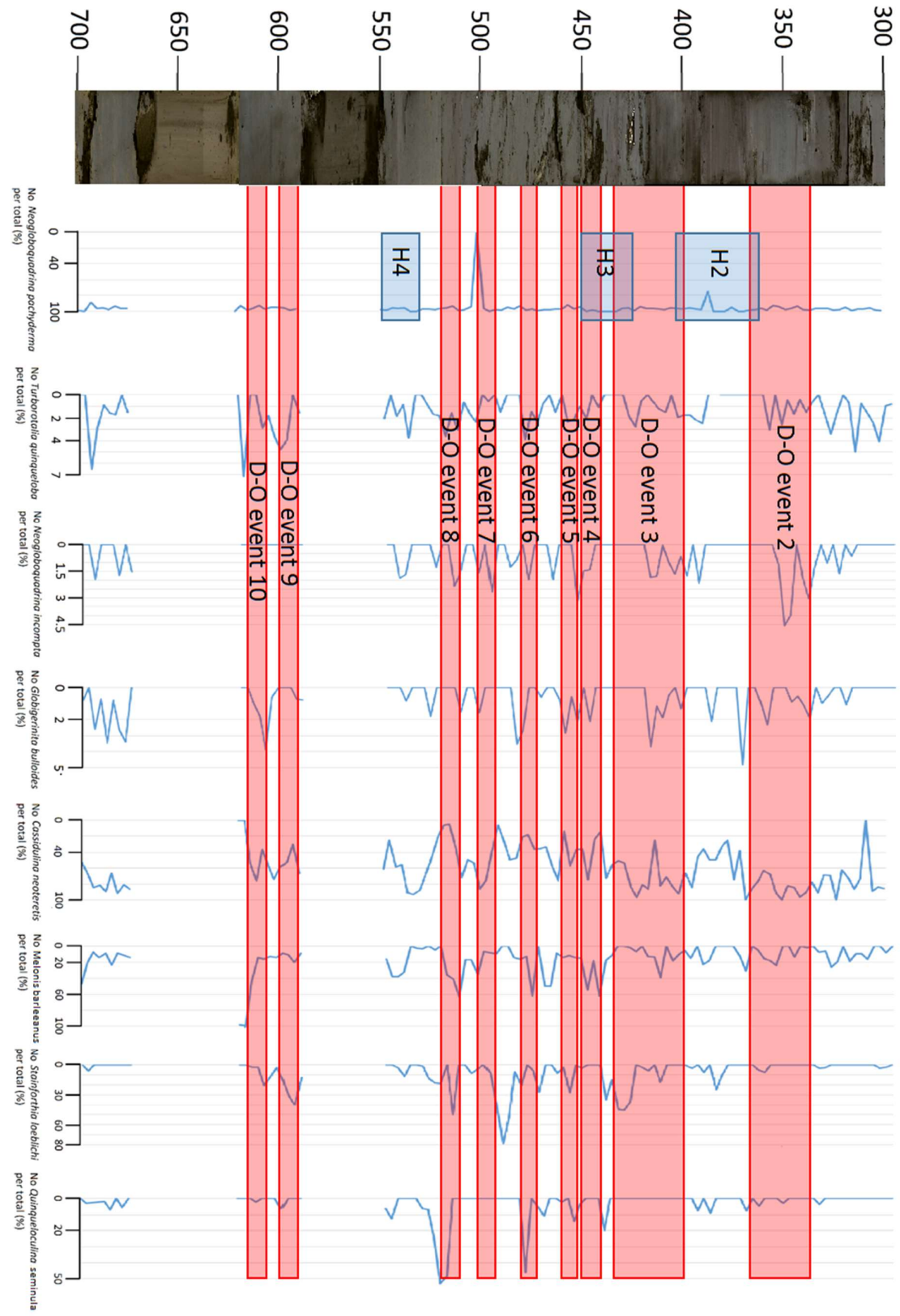

Figure 29: *Distribution of the most abundant planktic and benthic foraminifera plotted along the core. Dansgard-Oeschger events (red) and Heinrich events (blue) are highlighted.*

6 Conclusion

The position of the HH15-1255PC core in the Fram Strait allows the detailed analysis of climate changes during the Last Glacial Maximum. The climate in this area has been characterized by distinct temperature fluctuations described as Dansgaard-Oeschger events, as well as the occurrence of Heinrich events, which are layers of Ice Rafted Debris deposited in the North Atlantic.

By analyzing the core with different methods, it was possible to measure certain parameters. The ^{14}C dating of five samples gave an age for parts of the core. The core could be correlated with the core JM03-373PC2, that was previously described by Jessen et al. 2010.

Besides that, a debris flow event, which took place 23,440 ± 315 years ago, can be seen in both cores and provides information about the age. Afterwards an age model, that covers the period between 20,000 and 30,000 years, was established.

By comparing the foraminifera density with isotope measurements from the Greenland Ice Core, Dansgaard-Oeschger event 2 to 10 could be located in the HH15-1255PC core. Heinrich event 2, 3 and 4 were identified by comparing the 500 µm IRD fraction with detrital carbonate.

The focus was put on how the measured parameters and the distribution of different foraminifera species is changing during those events. The analysis gave following results:

- *Neogloboquadrina pachyderma* is the overall dominant species in the core. Their high abundance indicates that cold polar water has always been the main influence at the coring site.
- The most frequent benthic species is *Cassidulina neoteretis.* This species is linked to Atlantic-derived subsurface water. The influence of this water mass is varying over time, but mostly present during Dansgaard-Oeschger events.
- Other foraminifera species indicate changes in warm water inflow, organic supply, surges of ice sheet/expansion of sea ice during Dansgaard-Oeschger and Heinrich events. As well as the occurrence of the foraminifera species *Quinqueloculina seminula* in some samples, which is found in tidal-dominated environments, can be interpreted to be transported to the coring site by debris flow events or ocean currents.

The climatic changes, which happen during Dansgaard-Oeschger events, have a big influence on the distribution of foraminifera. The amount of the different species indicated how different

factors are varying. During Heinrich events, the conditions in the ocean are too turbulent for foraminifera species, but the IRD analysis indicate how strong the influence of this events was on the coring site.

References

- Aagaard K. and L. K. Coachman (1968): The East Greenland Current North of Denmark Strait: Part II, Arctic, Vol. 21, No. 4, pp. 269
- Alvarez-Solas J., Charbit S., Ritz C., Paillard D., Ramstein G. and Dumas C. (2010): Links between ocean temperature and iceberg discharge during Heinrich events, Nature Geoscience, Vol. 3, pp. 122
- Andersen K., Azuma N., Barnola J. M., Bigler M., Biscaye P. et al (2004): High-resolution record of Northern Hemisphere climate extending into the last interglacial period, Nature, 431, pp 147-150
- Andrews J. T. and Dunhill G. (2003): Early to mid-Holoce Atlantic water influx and deglacial meltwater events, Beaufort Sea slope, Arctic Ocean, Quaternary Research 61, pp. 468
- Armstrong H. (2009): Microfossils, Oxford: Blackwell publishing, pp. 142
- Bard E. (1988): Correction of accelerator mass spectrometry ^{14}C ages measured in planktonic foraminifera: Paleoceanographic implications, Paleoceanography, Vol. 3, 641
- Bard E., Hamelin B., Fairbanks R. G. and Zindler A. (1990): Calibration of the ^{14}C timescale over the past 30.000 years using mass spectrometric U-Th ages from Barbados corals, Nature, Vol. 345, pp. 407
- Bond G., Broecker W., Johnsen S., McManus J., Labeyrie L., Jouzel J., and Bonani G. (1993): Correlations between climate records from North Atlantic sediments and Greenland ice, Nature, Vol. 365, pp. 143, 146, 147
- Bourke R. H., Weigel A. M. and Paquette R. G. (1988): The Westward Turning Branch of the West Spitsbergen Current, Journal of Geophysical Research, Vol. 93, No. C11, pp. 14.065
- bouwmadesign.com, (2018). Arctic Biogeochemistry. [online] Available at: http://www.bouwmadesign.com/kostka/research/arctic/arctic.html [Accessed 13 June. 2018].)
- Bowman S. (1990): Radiocarbon Dating, The Trustees of the British Museum, pp. 10-12

- Braun H., Christl M., Rahmstorf S., Ganopolski A., Mangini A., Kubatzki C., Roth K. and Kromer B. (2005): Possible solar origin of the 1.470-year glacial climate cycle demonstrated in a coupled model, Nature, Vol. 438, pp.208
- Broecker W., Bond G. Klas M., Clark E. and McManus J. (1991): Origin of the northern Atlantic's Heinrich events, Climate Dynamics 6, pp. 265, 267
- Broecker W. (1997): Therohaline Circulation, the Achilles Heel of Our Climate System: Will Man-Made CO2 Upset The Current Balance**?**, Science, Vol. 278, pp 1528
- Bünz S., Polyanov S., Vadakkepuliyambatta S., Consolaro C. and Mienert J. (2012): Aktive gas venting through hydrate-bearing sediments on the Vestnesa Ridge, offshore W-Svalbard, Elsevier, Marine Geology 332-334 (2012), pp. 190
- Cacho I., Grimalt J., Pelejaro C., Canals M., Francisco J., Flores J. and Shackleton N. (1999): Dansgaard-Oeschger and Heinrich evet imprints in Aboran Sea paleotemperatures, Paleoceanography, Vol. 14, No. 6, pp. 698
- Corliss B. (1985): Microhabitats of benthic foraminifera within deep-sea sediments, Nature 314, pp. 435
- Darling K. F., Kucera M., Kroon D. and Wade C. M. (2006): A resolution for the coiling direction paradox in *Neogloboquadrina pachyderma*, Paleoceanography, Volume 21, pp. 1
- data.giss.nasa.gov, (2018). Global Seawater Oxygen-18 Database. [online] Available at: https://data.giss.nasa.gov/o18data/ [Accessed 14 June. 2018].
- Dokken T. and Hald M. (1996): Rapid climatic shifts during isotope stages 2-4 in the Polar North Atlantic, Geology, pp. 599
- Dowdeswell J. A., Maslin M. A., Andrews J. T. and McCave I. N. (1995): Iceberg production, debris rafting, and the extent and thickness of Heinrich layers (H-1, H-2) in North Atlantic sediments, Geology, v. 23 no. 4, pp. 301
- Elberling B., Knudsen K. L., Kristensen P. H. and Asmund G. (2002): Applying foraminiferal stratigraphy as a biomarker for heavy metal concentamination and mining impact in a fiord in West Greenland, Marine Environmental Research 55, pp. 245
- Elverhøi A., Andersen E. S., Dokken T., Hebbeln D., Spielhagen R., Svendsen J. I., Sørflaten M., Rørnes A., Hald M. and Forsberg C. F. (1995): The growth and decay of the Late Weichselian Ice Sheet in western Svalbard and adjacent areas based on provenance studies of marine sediments, Quaternary Research 44, 303-316
- geo.uni-bremen.de, (2017). Holocene variability in the Arctic gateway. [online] Available at: https://www.geo.uni-bremen.de/Interdynamik/index.php_FRAG_option

=com_content_AMP_task=view_AMP_id=35_AMP_Itemid=60 [Accessed 13 June. 2018].

- Grootes P. M., Stulver M., White J. W. C., Johnsen S. and Jouzel J. (1993): Comparison of oxygen isotope records from the GISP2 and GRIP Greenland Ice cores, Nature Vol. 366, pp. 552-553
- Haugan P. (1999): Structure and heat content of the West Spitsbergen Current, Polar Research 18 (2), pp. 183
- Hayward B. W. (1981): Foraminifera in nearshore sediments of the Eastern Bay of Islands, Northern New Zealand, Tane 27, pp. 123
- Hemming A. (2004): Heinrich events: Massive late Pleistocene detritus layers of the North Atlantic and their global climate imprint, Reviews of Geophysics, Vol. 42, 2-3
- Hopkins T. S. (1991): The GIN Sea – A synthesis of its physical oceanography and literature reviw 1972-1985, Earth-Science Reviews, vol. 30, pp. 176, 202
- Jessen S. P., Rasmussen T. L., Nielsen T., Solheim A. (2010): A new Late Weichselian and Holocene marine chronology for the western Svalbard slope 30,000-0 cal years BP, Quaternary Science Reviews 29, pp. 1305
- Jones G. A. and Keigwin L. D. (1988): Evidence from Fram Strait (78° N) for early deglaciation, Nature, Vol. 336, pp. 56-58
- Knudsen K. L. (1984): Foraminiferal stratigraphy in a marine Eemian-Weichselian sequence at Apholm, North Jutland, Bulletin of the Geological Society of Denmark, vol. 32, pp. 170
- Kohfeld K. E., Fairbanks R. G. (1997): *Neogloboquadrina pachyderma* (sinistral coiling) as paleoceanographic tracers in polar oceans: Evidence from Northeast Water Polynya plankton tows, sediment traps, and surface sediments, Paleoceanography, Vol. 11, No. 6, pp. 679
- Landvik J., Bondevik S., Elverhøi A., Fjeldskaar W., Mangerud J., Salvigsen O., Siegert M. J., Svendsen J. and Vorren T. (1998): The last glacial maximum of Svalbard and the Barents Sea Area: Ice sheet extent and configuration, Pergamon, pp. 56
- Lembke L., Tiedermenn R., Nürnberg D., Biebow N. and Kaiser A. (2003): Benthic foraminiferal C-13 anomalies in the Okhotsk Sea: evidence for Holocene methane dissociation events, EGS – AGU – EUG Joint Assembly
- Lynch-Stieglitz J., Adkins J. F., Curry W. B. et al (2018): Atlantic Meridional Overturning Circulation during the last Glacial Maximum, Science, Vol. 316, pp. 66

- Mackensen A., Sejrup H. P. and Jansen E. (1985): The distribution of living benthic foraminifera on the continental slpe and rise off southwest Norway, Elsevier, Volume 9, pp. 275
- McManus J. F., Francois R., Gherardi J. M., Keigwin L. D. and Brown-Leger S. (2004): Collapse and rapid resumption of Atlantic meridional circulation linked to deglacial climate changes, Nature, Vol. 238, pp. 834-836
- McMillen K., Warme J. E. and Hemmen E. H. (1977): An Electro-Osmotic Knife for Slicing Large Box Cores, Journal of Sedimentary Petrology, Vol. 47, No 2, pp. 864
- Müller J., Massé G., Stein R. and Belt S. (2009): Variability of sea-ice conditions in the fram Strait over the past 30,000 years, Nature Geoscience 2, pp. 772-773
- ncdc.noaa,gov, (2018). Heinrich and Dansgaard-Oeschger Events. [online] Available at: https://www.ncdc.noaa.gov/abrupt-climate- change/Heinrich%20and%20Dansgaard%E2%80%93Oeschger%20Events [Accessed 14 June. 2018]
- Nesje A. (1992): A Piston Corer for Lacustrine and Marine Sediments, Arctic and Alpine Research, Voln 24, No. 3, 1992, pp. 257
- Ohtsuka S., Suzaki T., Horiguchi T., Suzuki N. and Not F. (2015): Marine Protists – Diversity and Dynamics, Springer, pp. 129-130
- Pierre C. and Fouquet Y. (2007): Authigenic carbonated from methane seeps of the Congo deep-sea fan, Geo-Marine Letters, Volume 27, pp. 1
- Plaza-Faverola A., Bünz S., Johnson E., Chand S., Knies J., Mienert J. and Franek P. (2015): Role of tectonic stress in seepage evolution along the gas hydrate-charged Vestnesa Ridge, Fram Strait, Geophys. Res. Lett., 42, pp. 733-734
- Przybylak R., Araźny A. and Kejna M. (2012): Topoclimatic diversity in Forlandsundet region (NW Spitsbergen) in global warming conditions, Turpress, pp. 19
- Quadfasel D., Rudels B. and Kurz K. (1988): Outflow of dense water from a Svalbard fjord into the Fram Strait, Deep-Sea Research, Vol. 35, pp. 1148
- Rahmstorf S. (2002): Ocean circulation and climate during the past 120,000 years, Nature, Vol. 419, pp. 210
- Rasmussen T., Thomasen E., Ślubowska M. A., Jessen S., Solheim A. and Koç N. (2007): Paleoceanograpgic evolution of the SW Svalbard margin (76ºC) since 20.000 ^{14}C yr BP, Quaternary Research 67, 100-110
- Rasmussen T., Thomasen E., Skibekk K., Ślubowska-Woldengen M., Klitgaard K. and Koç K. (2013): Spatial and temporal distribution of Holocene temperature maxima in

the northern Nordic seas: interplay of Atlantic-, Arctic- and polar water masses, Quaternary Science Reviews 92, pp. 280

- Ravelo A. C., Hillaire-Marcel C. (2007): The Use of Oxygen and Carbon Isotopes of Foraminifera in Paleoceanography, pp. 735-745
- researchgate.net, (2018). Researchgate. [online] Available at: https://www.researchgate.net/figure/Locations-of-ice-core-sections-used-in-this-study-Sections-from-the-Greenland-Ice-Sheet_fig1_262384926 [Accessed 14 June. 2018].
- Richter T., Van der Gaast S., Koster B., Vaars A., Gieles R., De Stiger H., De Haas H. and Van Weering T. (2006): The Avaatech XRF Core Scanner: technical description and applications to NE Atlantic sediments, New Techniques in Sediment Core Analysis, pp. 39-40
- Ruddiman W. (1977): Late Quaternary deposition of ice-rafted sand in the subpolar North Atlantic (lat 40° to 69 N), Bulletin, Volume 88, Number 12, pp. 1813-1815
- Rudels B., Fahrbach E., Meincke J., Budéus G. and Eriksson P. (2002): The East Greenland Current and its contribution to the Denmark Strait overflow, ICES Journal of Marine Science, Volume 59, pp 1133
- Rundel P. W., Ehleringer J. R. and Nagy K. A. (1989): Stable Isotopes: History, Units and Instrumentation, Springer-Verlag, pp. 2-3
- Schäfer P., Ritzrau W., Schlüter M. and Tiede J. (2001): The Northern North Atlantic, Springer, pp.
- Schauer U., Fahrbach E., Osterhus S. and Rohardt G. (2004): Arctic warming through the Fram Strait: Oceanic heat transport from 3 years of measurements. Journal of Geophysical Research, pp. 327
- Sherwood Lollar B., Slater G. F., Ahad J., Sleep B., Spivack J., Brennan M. and MacKenzie P. (1999): Contrasting carbon isotope fractionation during biodegradation of trichloroethylene and toluene: Implications for intrinsic bioremediation, Organic Geochemistry 30, pp. 814
- Spalding K. L., Buchholz B. A., Bergman L., Druid H. and Frisén J. (2005): Forensics: Age written in teeth by nuclear tests, Nature 437, 333-334
- Spero H. J., Bijma J., Lea D. W. and Bemis B. E. (1997): Effect of seawater carbonate concentration on foraminiferal carbon and oxygen isotopes, Nature, Vol. 390, pp. 497
- Spero H. J. and Lea D. W. (1995): Experimental determination of stable isotope variablility in Globigerina bulloides: implications for paleoceanographic reconstructions, Marine Micropaleontology 28, pp. 231

- spscientific.com, (2018). Basic Principles of Freeze Drying. [online] Available at: https://www.spscientific.com/freeze-drying-lyophilization-basics/ [Accessed 13 June. 2018].
- Svendsen J. I., Alexanderson H., Astakhov V. I., Demidov I., Dowdeswell A., Funder S. Gataullin V., Henriksen M., Hjort C., Houmark-Nielsen M., Hubberten H. W., Ingólfsson Ó., Jakobsson M., Kjær K. H., Larsen E., Lokrantz H., Pekka Lunkka J., Lysá A., Mangerud J., Matiouchkov A., Murray A., Möller P., Niessen F., Nikolskaya O. Polyak L., Saarnisto M., Siegert C., Siegert M. J., Spielhagen R. F., Stein R. (2004): Late Quaternary ice sheet history of northern Eurasia, Quaternary Science Reviews 23, pp. 1230
- Talma A. and Vogel J. C. (1993): A simplified approach to calibrating 14C dates, The American Journal of Science, pp. 317
- thatslifesci.com, (2016). Estimating the Age of Life Long-Gone. [online] Available at http://thatslifesci.com.s3-website-us-east-1.amazonaws.com/2016-12-12-estimating-the-age-of-life-long-gone-dalcott/ [Accessed 14 June 2018]
- uit.no, (2018). Core Liner Saw. [online] Available at: https://uit.no/om/enhet/artikkel?p_document_id=390279&p_dimension_id=88137&men=28927 [Accessed 13 June 2018]
- uit.no, (2018). FF Helmer Hanssen. [online] Available at: https://uit.no/forskning/art?p_document_id=336568&dim=179012 [Accessed 26.04.2018]
- uit.no, (2018). MSCL with spectrophotometer. [online] Available at: https://uit.no/om/enhet/artikkel?p_document_id=390245&p_dimension_id=88137 [Accessed 13 June 2018]
- uit.no, (2016). Stable Isotope Laboratory. [online] Available at: https://site.uit.no/sil/analytical-services/ [Accessed 14 June, 2018].
- uit.no, (2017). X-Ray instrument. [online] Available at: https://uit.no/om/enhet/artikkel?men=28927&p_document_id=390469&p_dimension_id=88137 [Accessed 13 June 2018]
- uit.no, (2018). XRF core scanner container lab. [online] Available at: https://uit.no/om/enhet/artikkel?p_document_id=389557&p_dimension_id=88137 [Accessed 13 June 2018]
- Van Kreveld S., Sarntheim M., Erlenkeuser H., Grootes P., Jung S., Nadeau M. J., Pflaumann U. and Voelker A. (2000): Potential links between surging ice sheets,

circulation changes and the Dansgaard-Oeschger cycles in the Irminger Sea, 60-18 kyr, Paleoceanography, Vol. 15, No. 4, pp. 425-426, 437

- Vidal L., Labeyrie L., Cortijo E., Arnold M., Duplessy J. C., Michel E., Becqué S. and van Weering T. C. E. (1997): Evidence for changes in the North Atlabtic Deep Water linked to meltwater surges during the Heinrich events, pp. 13
- Vogt P., Crane K., Sundvor E., Max M. D. and Pfirman S. L. (1994): Methane-generated pockmarks on young, thickly sedimented oceanic crust in the Arctic: Vestnesa ridge, Fram strait, GEOLOGY. pp. 255
- Wang G. and Sassa K. (2002): Pore-pressure generation and movement of rainfall-induced landslides: effects of grain size and fine-particle content, Engineering Geology 69, pp. 109, 123
- Weber M., Niessen F., Kuhn G. and Wiedicke M. (1996): Calibration and application of marine sedimentary physical properties using a multi-sensor core logger, Marine Geology 136, pp. 151-152
- Modified template for title pages available at www.vectorstock.com

Appendix A

Core: HH-1255PC - Lab data

cm	Wet+Bag	dry+bag	bag	63-100µm	100-500µm	0.5-1mm	>1mm	%water content
300	32.136	23.2184	s	0.45	0.72	0.37	3.52	27.74956435
301	42.647	30.1022	s					29.41543368
302	65.733	45.0679	s					31.43793833
303	43.096	29.9147	s	0.87	0.93	0.11	0.25	30.58590124
304	68.198	47.121	s					30.9055984
305	69.503	48.0714	s					30.8355035
306	61.55	42.6426	s	0.97	1.08	0.09	0.16	30.71876523
307	61.522	42.5692	s					30.80654075
308	39.006	26.9507	s					30.90627083
309	45.007	31.1524	s	0.72	0.75	0.02	0.28	30.7832115
310	26.556	18.6329	s					29.83544208
311	39.89	27.89	s					30.0827275
312	44.264	31.8565	s	0.6	0.77	0.22	4.84	28.03067956
313	35.95	25.3654	s					29.44255911
314	34.484	24.7924	s					28.10462823
315	24.482	17.6689	s	0.29	0.49	0.15	1.24	27.82901724
316	30.93	22.9086	s					25.93404462
317	23.916	17.3686	s					27.37665161
318	46.696	32.9278	s	0.66	0.94	0.08	0.69	29.48475244
319	35.433	27.1153	s					23.47444473
320	39.076	29.4176	s					24.71696182
321	29.912	21.5482	s	0.46	0.79	0.06	0.74	27.9613533
322	63.959	47.4186	s					25.86094217
323	33.735	25.0683	s					25.69052912
324	25.62	18.9504	s	0.42	0.71	0.13	1.76	26.03278689
325	23.721	18.1325	s					23.55929345
326	28.356	21.596	s					23.83975173
327	25.185	18.2362	s	0.47	0.51	0.06	0.74	27.5910264
328	54.064	40.5278	s					25.03736313
329	43.251	30.7122	s					28.99077478
330	73.58	51.4165	s	1.58	1.43	0.14	0.92	30.12163631
331	44.6334	32.5362	m					27.1034696
332	47.5846	34.0822	m					28.37556689
333	49.091	34.8489	m	0.63	0.91	0.07	0.16	29.01163146
334	64.4714	44.8997	m					30.35718163
335	46.7019	32.3309	m					30.77176732
336	49.0112	34.4475	m	0.7	1.05	0.11	0.21	29.71504472
337	52.8437	36.1941	m					31.5072563
338	50.3284	34.5549	m					31.34115132
339	40.1062	29.1607	m	0.5	0.64	0.12	4.81	27.29129162
340	33.3832	23.6245	m					29.23236838
341	22.6784	16.2206	m					28.47555383
342	23.2956	16.8357	m	0.22	0.36	0.05	0.25	27.73012929
343	31.3502	22.5373	m					28.11114443
344	34.7422	24.8061	m					28.59951298
345	56.5425	39.4867	m	0.94	1.19	0.13	1.13	30.16456648

346	48.4833	33.5173	m					30.86836086
347	67.4078	46.6085	m					30.85592469
348	48.6339	34.5174	m	0.51	0.76	0.06	0.24	29.02604973
349	63.6329	44.1791	m					30.57192113
350	47.8696	33.7401	m					29.51664522
351	61.1019	43.4635	m	1.19	2.01	0.15	0.35	28.86718744
352	73.5168	52.7179	m					28.29135653
353	53.3102	37.8499	m					29.00064153
354	60.8821	42.5553	m	1.49	1.5	0.06	0.09	30.1021154
355	59.457	41.0227	m					31.00442336
356	55.4303	37.7079	m					31.97240498
357	55.6576	37.3522	m	0.2	0.19	0	0	32.88930892
358	54.4065	36.4658	m					32.97528788
359	72.2295	48.0904	m					33.42000152
360	52.7271	35.5503	m	0.28	0.22	0.01	0	32.57679637
361	44.6477	30.5412	m					31.59513256
362	63.9657	44.2124	m					30.88108158
363	59.6574	41.9832	m	0.67	0.89	0.11	0.4	29.6261654
364	56.2309	39.9733	m					28.9122173
365	57.6524	41.4958	m					28.02415858
366	53.8431	39.1492	m	1	2.09	0.22	0.88	27.29021917
367	75.7802	55.0931	m					27.29881948
368	53.8609	40.8675	m					24.12399347
369	82.8595	64.2192	m	2.91	6.72	0.98	2.64	22.49627381
370	66.1192	51.7179	m					21.78081404
371	70.7394	55.0836	m					22.13165506
372	74.5574	57.8219	m	2.77	4.46	0.5	1.99	22.44646407
373	64.6324	50.9325	m					21.19664441
374	91.3471	72.0447	m					21.13082955
375	69.6824	55.1539	m	2.9	5.02	0.57	1.15	20.8495976
376	100.9239	78.1439	m					22.57146226
377	88.1904	67.8313	m					23.08539251
378	99.1829	77.0266	m	3.7	5.7	0.76	2.24	22.33883058
379	95.5565	74.0164	m					22.54174232
380	70.2382	55.2826	m					21.29268689
381	92.5327	73.2668	m	3.32	5.31	0.69	7.7	20.82063962
382	90.5124	70.0698	m					22.58541371
383	76.6972	58.1576	m					24.17246001
384	73.6992	56.4817	m	1.82	3.6	0.43	0.5	23.36185467
385	74.5257	56.3693	m					24.36260243
386	114.4692	86.4469	m					24.48020952
387	60.9224	46.1189	m	2.18	1.22	0.34	1.13	24.29894423
388	94.9526	71.0888	m					25.13232918
389	100.2717	73.4918	m					26.70733617
390	62.8505	47.1052	m	1.01	1.77	0.3	1.9	25.05198845
391	91.6705	70.1	m					23.53047054
392	71.7494	54.5345	m					23.99309263

393	69.4951	50.9358	m	0.95	1.62	0.25	0.68	26.70591164
394	60.2151	44.3417	m					26.3611619
395	67.2115	49.0682	m					26.99433877
396	57.6943	41.9906	m	0.52	0.87	0.1	0.72	27.21880671
397	56.1312	40.9981	m					26.96022889
398	58.0678	42.6607	m					26.53294941
399	66.0365	47.9092	m	1.03	1.61	0.14	0.81	27.45042514
400	55.7997	39.1569	m					29.82596681
401	47.1952	32.6659	m					30.78554599
402	40.4088	28.0463	m	0.23	0.19	0.01	0.02	30.59358358
403	57.5686	39.6846	m					31.06554615
404	65.3097	45.0335	m					31.0462305
405	44.4482	28.9811	m	0.49	0.45	0.03	0.11	34.79803457
406	90.2966	70.6611	m					21.74555853
407	47.4426	34.9058	m					26.42519592
408	64.3728	46.8217	m	1.33	1.59	0.11	0.24	27.26477643
409	66.523	48.2544	m					27.46208078
410	62.5896	45.5821	m					27.17304472
411	65.9774	48.5015	m	1.42	1.79	0.11	0.31	26.4877064
412	64.2604	46.9927	m					26.87144805
413	57.6495	41.2876	m					28.38168588
414	79.0192	55.8485	m	1.06	0.74	0.08	0.14	29.32287343
415	55.7092	39.3767	m					29.31741974
416	52.3746	37.3115	m					28.76031511
417	43.6833	31.7014	m	0.33	0.59	0.24	2.08	27.4290175
418	61.0842	43.1952	m					29.28580549
419	71.5001	50.8485	s					28.88331625
420	86.9695	61.8483	s	0.65	0.79	0.04	0.11	28.8850689
421	82.3017	57.8106	s					29.75770853
422	62.1461	43.3506	s					30.24405393
423	54.3019	37.8918	s	0.33	0.27	0.04	0.07	30.22012121
424	85.3228	59.1094	s					30.72262045
425	64.7833	45.8325	s					29.25260059
426	55.1719	39.8141	s	0.97	1.03	0.02	0.32	27.83627173
427	69.0426	49.9381	s					27.67059757
428	78.1176	56.9186	s					27.13729044
429	84.1504	62.2374	s	1.09	1.17	0.11	0.26	26.04028026
430	83.1404	62.2906	s					25.07782017
431	61.4776	46.6419	s					24.13187893
432	105.8984	81.2537	s	0.39	0.65	0.13	1.14	23.272023
433	73.0406	56.5227	s					22.61468279
434	99.1701	76.544	s					22.81544538
435	51.1267	39.376	s	0.3	0.29	0.04	0.11	22.98349004
436	101.8309	77.3034	s					24.08650027
437	85.739	63.5815	s					25.84296528
438	64.5532	47.3534	s	1.2	1.1	0.11	0.15	26.64438014
439	95.5247	70.716	s					25.97097923

440	40.6807	30.4708	s					25.09765073
441	83.0352	61.9664	s	0.84	2.69	0.27	0.79	25.37333565
442	77.8434	56.3789	s					27.57394975
443	48.0424	34.6923	s					27.78816212
444	55.6965	39.82	s	0.62	0.53	0	0.09	28.50538185
445	45.0781	31.94	s					29.14519467
446	27.7431	19.6798	s					29.0641637
447	53.8604	38.2894	s	0.59	0.63	0.1	2.35	28.90992269
448	54.3373	38.3237	s					29.47073189
449	56.9597	39.2982	s					31.00701022
450	41.0501	28.3547	s	0.3	0.35	0.04	0.1	30.92659945
451	51.6673	35.4714	s					31.34651898
452	56.3179	38.7736	s					31.15226242
453	66.8935	46.0317	s	0.53	0.37	0	0.05	31.18658764
454	71.4278	49.0962	s					31.26457766
455	73.0251	50.1173	s					31.3697619
456	67.7025	46.4284	s	0.54	0.37	0	0.04	31.42291644
457	52.7012	36.4807	s					30.77823655
458	116.9254	80.1674	s					31.43713855
459	59.9355	41.7297	s	0.41	0.37	0.05	0.08	30.37565383
460	62.0024	43.4453	s					29.92964788
461	27.9377	19.9111	s					28.73035361
462	77.6949	55.2149	s	1.11	0.83	0.06	1.33	28.93368805
463	63.8494	45.1013	s					29.36300106
464	68.1833	47.1761	s					30.8098904
465	93.0195	63.688	s	0.67	0.44	0.02	0.1	31.53263563
466	89.4792	60.6288	s					32.24257705
467	47.2554	32.2331	s					31.78959442
468	54.6198	38.6319	s	0.37	0.42	0.01	0.02	29.27125328
469	65.2241	45.0179	s					30.97965323
470	97.0431	66.7246	s					31.24230368
471	50.8933	36.1648	s	0.53	0.51	0.06	3.01	28.9399587
472	67.2956	49.0687	s					27.0848317
473	91.8246	63.78	s					30.54148888
474	92.7408	63.4949	s	0.77	0.68	0.1	0.4	31.53509566
475	66.4137	45.2294	s					31.89748501
476	60.9116	41.595	s					31.71251453
477	90.2933	61.2975	s	0.49	0.73	0.04	0.06	32.11290317
478	72.8214	49.6929	s					31.76058137
479	79.2895	53.8479	s					32.08697242
480	91.613	62.2524	s	0.78	0.64	0.04	0.05	32.0485084
481	67.5209	46.0637	s					31.77860485
482	76.9934	52.3896	s					31.95572608
483	70.6634	48.2432	s	0.46	0.34	0.01	0.04	31.72816479
484	100.6712	69.5609	s					30.90287987
485	75.618	52.5414	s					30.51733714
486	73.9672	51.9489	s	0.85	0.94	0.07	0.37	29.76765377

487	61.4715	43.346	s					29.48602198
488	74.6412	52.0244	s					30.30069184
489	77.0793	53.0968	s	1.05	0.59	0	0.08	31.11406045
490	62.5862	43.3342	s					30.76077474
491	89.871	62.4594	s					30.50105151
492	71.5923	50.1912	s	0.89	0.89	0.14	0.28	29.89301922
493	58.2074	40.8873	s					29.7558386
494	99.0253	70.3337	s					28.97400967
495	65.1592	47.7327	s	2.33	0.8	0	0	26.74449656
496	84.5947	61.4184	s					27.39687002
497	41.0325	30.0633	s					26.73295558
498	33.759	24.2808	s	0.61	0.24	0.03	0.03	28.0760686
499	73.9105	51.4601	s					30.37511585
500	49.1828	34.3166	s					30.22642062
501	64.403	45.1799	s	0.32	0.21	0.03	0.06	29.84814372
502	93.8294	65.439	s					30.25746728
503	75.1565	52.7593	s					29.8007491
504	62.301	44.0475	s	0.24	0.13	0.01	0.02	29.29888766
505	76.3415	53.7071	s					29.64888036
506	59.6452	41.8025	s					29.9147291
507	79.9717	56.0642	s	0.51	0.35	0	0.01	29.89495034
508	53.1709	37.8207	s					28.86955083
509	52.1542	37.09	s					28.88396332
510	37.9559	27.1181	s	0.37	0.3	0.01	0.17	28.55366359
511	62.7997	44.2665	s					29.51160595
512	27.0641	19.6035	s					27.56640716
513	48.3609	36.914	s	0.38	0.42	0.03	6.55	23.66974146
514	58.904	42.2653	s					28.2471479
515	46.1809	33.6237	s					27.19132802
516	93.3023	66.9758	s	0.68	0.74	0.06	0.17	28.21634622
517	67.2437	47.0198	s					30.07553124
518	80.988	56.9315	s					29.70378328
519	72.6698	50.4628	s	0.48	0.36	0.05	0.15	30.55877407
520	90.2108	62.0633	s					31.20191817
521	59.5386	41.1226	s	0.4	0.36	0.03	0.05	30.93119422
522	98.3397	67.5082	s					31.35203789
523	76.1241	52.541	s					30.97980797
524	73.9474	51.6054	s					30.21336788
525	92.7796	63.8637	s	0.62	0.66	0.07	0.29	31.1662262
526	71.7718	49.5472	s					30.96564389
527	71.5183	49.4145	s					30.90649526
528	62.8907	43.5537	s	0.37	0.34	0.06	0.15	30.74699439
529	75.7219	52.5199	s					30.64106949
530	74.1569	51.4364	s					30.63841665
531	52.8068	36.7586	s	0.36	0.26	0.03	0.13	30.39040427
532	71.5206	49.4897	s					30.80357268
533	74.6454	51.0822	s					31.56684806

534	65.9663	45.3749	s	0.57	0.68	0.06	0	31.21502949
535	84.2057	58.7682	s					30.20876259
536	65.8098	46.0498	s					30.02592319
537	83.3992	57.6647	s	0.85	0.9	0.1	0.19	30.85701062
538	78.9079	54.3487	s					31.12387987
539	47.9118	33.2463	s					30.60936972
540	89.0607	61.5501	s	0.91	0.94	0.12	0.39	30.88971903
541	69.3765	48.5539	s					30.01390961
542	67.585	47.4345	s					29.81504772
543	64.9479	45.7409	s	0.68	0.85	0.09	0.29	29.57293461
544	45.2273	31.7654	s					29.76498708
545	47.6522	33.2817	s					30.15705466
546	65.8207	45.7099	s	0.5	0.54	0.02	0.31	30.55391389
547	33.6341	24.004	s					28.63195388
548	16.4834	11.9415	s					27.55438805
549	17.6048	12.7739	s	0.18	0.18	0	0.01	27.4408116
588	75.0343	53.623	s					28.53534983
589	63.4851	45.8945	s					27.7082339
590	70.3006	50.9489	s	0.97	0.85	0.02	0.5	27.52707658
591	64.7399	46.7469	s					27.79275223
592	47.838	34.8467	s					27.15686275
593	68.8521	50.1587	s	0.67	0.57	0.08	1.61	27.15007966
594	61.0467	44.8221	s					26.57735799
595	71.9223	52.6253	s					26.8303433
596	63.7531	47.0171	s	1.18	0.85	0.14	0.02	26.25127249
597	78.0823	57.9786	s					25.74680818
598	67.4292	49.9127	s	1.35	0.87	0.05	0.13	25.97761801
599	45.9438	33.5783	s					26.91440412
600	47.3877	34.5344	s					27.1237051
601	74.8841	54.1624	s					27.67169533
602	58.6433	42.7684	s	0.6	0.29	0.01	0	27.0702706
603	60.8574	44.3709	s					27.09037849
604	53.414	38.709	s					27.53023552
605	60.4165	43.3319	s	0.61	0.08	0	0.01	28.27803663
606	61.3045	43.4585	s					29.11042419
607	66.0892	46.5751	s					29.52691211
608	45.131	31.883	s	0.22	0.06	0.01	0	29.35454566
609	59.5963	41.8312	s					29.80906533
610	61.8297	43.7682	s					29.21168953
611	70.1998	49.8624	s	0.49	0.39	0.01	0	28.97073781
612	52.1634	37.4681	s					28.17166826
613	70.663	50.6334	s					28.34524433
614	25.297	18.3854	s	0.35	0.46	0.01	0	27.32181682
615	34.1381	24.5952	s					27.95381114
616	51.3445	37.0761	s					27.78953929
617	59.6957	42.8414	s	0.64	0.46	0.01	0.12	28.23369187
618	38.829	27.9041	s					28.13592933

669	31.5134	22.1355	s					29.75845196
671	41.1406	28.5839	s	0.2	0.29	0	0.01	30.52143138
672	57.9391	40.1164	s					30.76109225
673	68.3568	48.7908	s					28.62334106
674	77.8232	54.0294	s	0.41	0.61	0.05	0.23	30.57417325
675	81.4042	56.8297	s					30.18824582
676	56.5617	39.0483	s					30.96335506
677	61.4485	42.1743	s	0.35	0.22	0.01	0.04	31.3664288
678	92.8511	62.9679	s					32.18400213
679	52.997	36.066	s					31.94709134
680	50.4791	34.4662	s	0.7	0.15	0	0.03	31.72184132
681	76.2835	51.7136	s					32.20866898
682	57.967	39.5637	s					31.74789104
683	77.8492	53.0989	s	0.4	0.35	0	0	31.79261958
684	69.5007	47.7498	s					31.29594378
685	65.9665	45.2827	s					31.35500595
686	71.6271	48.8899	s	1.22	0.76	5.64	0.01	31.74385114
687	47.3902	32.3541	s					31.72828982
688	47.0198	32.1662	s					31.59009609
689	33.1492	22.9285	s	0.19	0.18	0	0.06	30.83241828
690	24.9894	17.3743	s					30.47332069
693	50.254	34.4639	s					31.42058344
694	34.6255	23.9368	s	0.45	0.59	0.08	0.04	30.86944593
695	40.6187	27.8574	s					31.41730287
696	39.6655	27.1426	s					31.5712647
697	37.0722	26.1506	s	0.39	0.76	0.07	4.9	29.46035034
698	66.4859	45.2113	s					31.99866438
699	61.7031	42.3407	s					31.37994687

cm	Tot. dry weight	No. Planktic	No. Benthic	Squares counted for planktic	Squares counted for benthic	weight res. On tray
300	0.72	129	17	25	45	0.36
303	0.93	218	38	15	15	0.23
306	1.08	195	37	8	20	0.49
309	0.75	161	51	10	15	0.39
312	0.77	133	21	5	10	0.77
315	0.49	134	32	17	45	0.49
318	0.94	100	11	27	27	0.94
321	0.79	151	49	10	25	0.41
324	0.71	94	14	18	18	0.39
327	0.51	121	28	25	45	0.25
330	1.43	178	20	10	15	0.69
333	0.91	189	46	10	13	0.42
336	1.05	102	31	12	12	0.49
339	0.64	213	32	11	11	0.35
342	0.36	262	58	7	15	0.36
345	1.19	261	36	5	5	0.6
348	0.76	177	23	5	15	0.39
351	2.01	235	49	5	5	0.5
354	1.5	263	48	5	10	0.65
357	0.19	177	46	10	20	0.19
360	0.22	131	11	7	15	0.22
363	0.89	171	42	10	15	0.41
366	2.09	202	19	10	15	2.09
369	6.72	160	29	20	20	0.28
372	4.46	87	10	45	45	2.1
375	5.02	62	11	45	45	1.25
378	5.7	22	4	45	45	0.61
381	5.31	10	11	45	45	0.77
384	3.6	40	10	45	45	0.43
387	1.22	12	10	45	45	0.33
390	1.77	47	10	45	45	0.885
393	1.62	158	17	20	20	0.85
396	0.87	91	14	20	20	0.42
399	1.61	168	36	29	29	0.99
402	0.19	112	116	10	10	0.19
405	0.45	151	38	10	10	0.45
408	1.59	239	35	5	15	0.78
411	1.76	197	22	10	10	0.89
414	0.74	160	39	6	10	0.39
417	0.59	166	36	10	20	0.26
420	0.79	228	18	5	5	0.35
423	0.27	183	40	10	10	0.27
426	1.03	105	37	10	20	0.39
429	1.17	108	120	16	16	0.55
432	0.65	108	98	35	35	0.3
435	0.29	69	82	45	45	0.29

438	1.1	101	32	45	45	1.1
441	2.52	63	78	32	32	0.65
444	0.53	188	37	5	15	0.53
447	0.63	194	32	14	45	0.3
450	0.3	141	16	23	30	0.3
453	0.35	198	42	20	35	0.35
456	0.37	93	11	6	6	0.37
459	0.37	169	44	30	30	0.37
462	0.83	138	81	15	15	0.46
465	0.44	130	43	10	10	0.44
468	0.42	102	17	14	32	0.21
471	0.51	130	35	20	40	0.51
474	0.68	167	29	15	17	0.28
477	0.73	135	17	21	21	0.31
480	0.64	102	28	20	20	0.64
483	0.34	111	29	20	35	0.34
486	0.94	112	15	10	10	0.44
489	0.59	157	23	15	15	0.59
492	0.89	131	59	22	22	0.43
495	0.8	114	63	8	8	0.38
498	0.24	187	88	13	13	0.24
501	0.21	113	49	20	20	0.21
504	0.31	126	56	15	20	0.31
507	0.35	171	31	15	15	0.35
510	0.3	162	23	35	35	0.3
513	0.42	131	9	12	12	0.42
516	0.74	127	30	3	6	0.32
519	0.36	109	41	20	20	0.36
521	0.36	109	37	15	15	0.36
525	0.66	233	56	24	24	0.32
528	0.34	111	47	14	14	0.34
531	0.26	121	71	20	20	0.26
534	0.68	116	49	20	20	0.68
537	0.9	106	19	45	45	0.45
540	0.94	118	54	22	40	0.42
543	0.85	210	34	15	15	0.41
546	0.54	86	11	8	8	0.54
549	0.18	144	45	35	45	0.18
590	0.85	127	27	25	25	0.46
593	0.57	135	20	14	21	0.57
596	0.85	102	25	15	15	0.38
598	0.87	104	55	21	21	0.41
599	0.33	108	45	13	13	0.33
602	0.29	162	42	24	24	0.29
605	0.08	102	45	33	33	0.08
608	0.06	112	44	15	15	0.06
611	0.39	102	48	40	40	0.39

614	0.46	28	20	45	45	0.46
617	0.46	43	71	45	45	0.28
671	0.29	103	32	35	35	0.29
674	0.61	117	59	5	15	0.31
677	0.22	131	25	15	15	0.22
680	0.15	128	53	10	10	0.15
683	0.35	115	44	5	5	0.35
686	0.76	139	52	20	20	0.35
689	0.18	153	76	22	22	0.18
694	0.59	113	39	35	35	0.59
697	0.76	114	17	36	45	0.33

Planktic Species						
cm	Neogloboquadrina pachyderma	Neogloboquadrina incompta	Turborotalia quinqueloba	Globigerinita uvula	Globigerinita bulloides	Globigerinita glutinata
300	128		1			
303	215		2	1		
306	187		8			
309	157		4			
312	129		2	2		
315	133		1			
318	95		5			
321	148	1	1	1		
324	93				1	
327	117	2	2			
330	85		3			
333	183	2	3		1	
336	101				1	
339	159	2	1			
342	245	8	4		5	
345	253	5	1		3	
348	173		3		1	
351	213	9	1		2	
354	244	12	7			
357	175	2				
360	127		4			
363	167				4	
366	199				2	1
369	160					
372	87					
375	59				3	
378	22					
381	10					
384	40					
387	9		3			
390	46				1	
393	154		4			
396	87	2	2			
399	164		3			1
402	108	2	2			
405	145	1	3		2	
408	235	4				
411	191	2	3		1	
414	155		2		3	
417	160	3	1		2	
420	102	2			4	
423	182		1			
426	101		3			1
429	104		2			2
432	108					
435	69					
438	101					
441	63					
444	186		2			
447	194					
450	133	2	3		3	
453	195	3	2			
456	86	3	2		2	
459	164		4		1	
462	102				3	
465	127		2		1	

444	186		2			
447	194					
450	133	2	3		3	
453	195	3	2			
456	86	3	2		2	
459	164		4		1	
462	102				3	
465	127		2		1	
468	100	2				
471	129		1			
474	162		4		1	
477	133		2			
480	96	2	4			
483	108				3	
486	107	1			4	
489	155	2				
492	128		2			1
495	114					
498	181	5	1			
504	119	2	3		2	
507	168		3			
510	161		1			
513	123	2	4		2	
516	122	3	2			
519	105		4			
521	107		2			
525	226	3	4			
528	108		1		2	
531	121					
534	110					
537	102		4			
540	114	2	1		1	
543	202	4	4			
546	85					1
549	141		3			
590	124		2		1	
593	133				1	1
596	98		4			
598	99		5			
599	103		4			1
602	158		3		1	
605	95		3		4	
608	108			2	2	
611	101				1	
614	26		2			
617	43					
671	127	2	2			
674	113				4	
677	107	2	2		3	
680	125		2		1	
683	110		1		4	
686	134		4		1	
689	136	3	10		4	
694	113					
697	113				1	

Benthic species																		
cm	Cassidulina	Cribroelphidium	Melonis	Cibides	Stainforthia	Hyalinea	Cibides	Cribroelphidium	Elphidium	Nanionellina	Cassidulina	Cribroelphidium	Triloculina	Quinqueloculina	Ammodiscus	Bolivinellina	Cibides	Hyperammina
300	12	2																
303	31		3	1	1	1												
306	25	1			1		1											
309																		
312	14		3					1	1									
315	19		2							1								
318	8		1								1	1						
321	20		6				2			2			2					
324	13																	
327	18	2	5			1												
330	13		5						1									
333	30		2		1													
336	21		2		1			1		1				1				
339	30						1		1						1			
342	59		1					1										
345	22							2		2								
348	19		3						1									
351	34																	
354	31						1		1					1				
357	28		10					3										
360	7		2				1	1										
363	30		6		3													
366	18		1		1									1				
369	26																	
372	5		4									2		1		1		
375	6		1				1											
378	1						1										2	
381	2			3													1	
384	5				1			1									3	
387	2	1			1													
390	4		2				3							1				1
393	6		3		1	3												
396	11								1					1				
399	18		4	1	1				2	1								
402	88		5				1	1										
405	26		3													2		
408	20		5						3									
411	14								2	1								
414	7		11		5		4		1									
417	26		4															
420	13		2		1													
423	33				1													
426	26		2					2	1									
429	53	2	2		37				5									
432	42	3			37													
435	36				29													
438	19		3		4													
441	6	2	7		14									8		3		
444	7		18				1		3									
447	21		5									2						
450	4		6													1		
453	10		4		1		1			9				1		1		
456	4		1					1						1				
459	5		4		10				1	15		1						
462	32		6		1		2							1				
465	14		2		2		1	4									1	

cm	Cassidulina	Cribroelphidium	Melonis	Cibides	Stainforthia	Hyalinea	Cibides	Cribroelphidium	Elphidium	Nanionellina	Cassidulina	Cribroelphidium	Triloculina	Quinqueloculina	Ammodiscus	Bolivinellina	Cibides	Hyperammina
468	4		6						1	1								
471	10		14							1			3					
474	8			6			1			5			1	1				
477	3		10	1						2								
480	5		3			1				4			11			1		
483	9		3	4					1	1								
486	7		2	1					2	2								
489	5			10		1			1	2								
492	3			37		1			4	2								
495	17	1	4	18					2									
498	47		5	5					5									
501	38		3	1			1		1									
504	23		15	2			2		1									
507	12		4	2			6											
510	13		3						1					1				
513	4		7															
516	1		9	11						1								
519	2		11						1				15			2		
521	7	1		6									17			1		
525	21		2	8						2			11					
528	20			4					1				2			2		
531	56		2	1		1							4					
534	42		1						2									
537	20						1		1									
540	24		14	5														
543	17		11	1														
546	2		3						2				1					
549	19		5				2		3				2					
590	16		2	3					1	2								
593	6		4	8			2											
596	10		2	6					1									
598	27		4	7						4			3	1				
599	26		5	1		1				2								
602	18		4	4					2	4								
605	7		3	4		3	1							1				
608	32		6	1		2							1					
611	21		17	1														
614			16															
617			71													1		
671	25		4															
674	43		6	1									3					
677	22		2															
680	28		10							1			3					
683	43		4										1					
686	35		6				1						1					
689	61		5				1						2	2		1		
694	23		7	2					1				1					
697	9		8															

Full name of benthic foraminifera found in the core HH15-1255PC:

Cassidulina neoteretis

Melonis barleeamis

Cibides wuellerstofi

Stainforthia loeblichi

Hyalinea balthica

Cibides lobatulus

Cribroelphidium incertum

Elphidium exacavatum

Nanionellina labradorica

Cassidulina laevigata

Cribroelphidium albiumbilicatum

Triloculina tricurinata

Quinqueloculina seminula

Ammodiscus sp.

Bolivinellina pseudopunctata

Cibides refulgens

Hyperammina sp.

Appendix B

Stable Isotope Laboratory

: Analysis report

Date:	10.03.2018
Job nr:	53 Part1
Sample type:	Forams
Nr of samples:	50
Analysis:	d13C, d18O in carbonates
Sample owners:	Felix (Tine Rasmussen)
Notes:	**Ran at T=40C instead of 50C**
Method:	No pre-treatment is performed, unless requested. Carbonate samples are placed in 4.5mL vials. The vials are flushed with He, and 5 drops of water free H3PO4 are added manually with a syringe. After equilibration >2h at T = 50C, the samples are analysed on Gasbench II and MAT253 IRMS. Normalisation to VPDB by 3 inhouse standards with d13C, d18O values that enclose the samples. The inhouse standards have been normalised by several international standards. Instrument uncertainty d13C, d18O is standard deviation ≤0.1 permil (ThermoScientific). Uncertainty in d13C, d18O for heterogeneous samples/small samples may be larger.
Instrument:	Thermo Scientific MAT253 IRMS + Gasbench II
Operator:	Matteus Lindgren: matteus.lindgren@uit.no
Reference:	**Please add the following reference in publications based on this data** The Stable Isotope Laboratory at CAGE – Centre for Arctic Gas Hydrate, Environment and Climate located at UiT – The Arctic University of Norway, in Tromsø, Norway Website http://site.uit.no/sil/

Normalisation Standards

d13C	Standard 1	Standard 2	Standard 3	Comment
TRUE d13C [‰ vs VPDB]	1.96	-10.21	-48.95	
Normalised avg d13C this run [‰ vs VPDB]	1.92	-10.15	-48.96	
Standard deviation [‰ vs VPDB]	0.04	0.02	0.05	Spec. ≤0.10
Nr of replicates	2	2	4	

Linear regression R2-value d13C	1.00000	Spec. >0.99950

d18O	Standard 1	Standard 2	Standard 3	Comment
TRUE d18O [‰ vs VPDB]	-2.15	-18.59		
Normalised avg d18O this run [‰ vs VPDB]	-2.15	-18.59		
Standard deviation [‰ vs VPDB]	0.04	0.08		Spec. ≤0.10
Nr of replicates	2	2		

Linear regression R2-value d18O	0.99997	Spec. >0.99950

Quality Control Samples

d13C	QC Sample 1	QC Sample 2	Comment
TRUE d13C [‰ vs VPDB]	2.67	-46.60	
Normalised avg d13C this run [‰ vs VPDB]	2.67	#N/A	
Standard deviation [‰ vs VPDB]	0.06	#N/A	Spec. ≤0.10
Nr of replicates	2	1	

d18O	QC Sample 1	QC Sample 2	Comment
TRUE d18O [‰ vs VPDB]	-1.40	-26.41	
Normalised avg d18O this run [‰ vs VPDB]	-1.54	#N/A	
Standard deviation [‰ vs VPDB]	0.17	#N/A	Spec. ≤0.10
Nr of replicates	2	2	

Samples

Sample name	Peak area [Vs]	d13C VPDB [‰]	d18O VPDB [‰]	Comment
77	18.54	-9.19	5.82	
76	21.89	-5.05	6.02	
75	78.77	-3.00	5.50	
74	33.85	-7.62	6.06	
73	87.20	-5.38	5.46	
72	43.84	-3.91	5.56	
71	21.87	-7.94	5.60	
90	66.69	-3.89	5.44	
89	41.00	-4.03	5.50	
88	23.88	-7.26	5.55	
87	34.31	-3.49	5.33	
86	45.41	-4.81	5.29	
85	28.98	-1.45	5.34	
84	83.17	-3.34	5.54	
83	61.54	-4.10	5.45	
82	39.54	-2.70	5.53	
81	93.56	-6.18	5.56	
100	75.72	-9.50	5.36	
99	55.45	-4.91	5.25	
98	46.19	-4.07	4.91	
97	68.62	-4.50	5.18	
96	47.73	-4.51	5.61	
95	37.55	-4.31	5.59	
94	78.86	-4.36	5.38	
93	60.35	-4.24	5.47	
92	81.54	-6.45	5.43	
91	23.88	-2.30	5.44	
60	95.97	-3.89	5.57	
59	30.66	-4.41	5.70	
58	32.10	-5.06	5.63	
57	45.76	-5.67	5.74	
56	38.93	-10.21	5.88	
55	85.65	-10.90	5.69	
54	117.64	-3.26	5.57	
53	71.85	-5.24	5.58	
52	31.12	-3.28	4.92	
51	40.74	-5.29	4.84	
70	32.93	-3.60	5.48	
69	24.00	-2.38	5.90	
68	26.64	-3.49	5.61	
67	31.21	-3.42	5.81	
66	13.48	-4.23	5.76	Small sample
65	62.03	-5.80	4.82	
64	38.34	-2.60	4.98	
63	52.25	-5.81	5.48	
62	22.35	-7.55	5.89	
61	102.36	-3.31	5.48	
80	30.62	-4.80	5.33	
79	95.06	-6.83	5.56	
78	53.92	-3.39	5.59	

Stable Isotope Laboratory

: Analysis report

Date:	11.03.2018
Job nr:	53 Part2
Sample type:	Forams
Nr of samples:	54
Analysis:	d13C, d18O in carbonates
Sample owners:	Felix (Tine Rasmussen)
Notes:	**Ran at T=40C, instead of 50C**
Method:	No pre-treatment is performed, unless requested. Carbonate samples are placed in 4.5mL vials. The vials are flushed with He, and 5 drops of water free H3PO4 are added manually with a syringe. After equilibration >2h at T = 50C, the samples are analysed on Gasbench II and MAT253 IRMS. Normalisation to VPDB by 3 inhouse standards with d13C, d18O values that enclose the samples. The inhouse standards have been normalised by several international standards. Instrument uncertainty d13C, d18O is standard deviation ≤0.1 permil (ThermoScientific). Uncertainty in d13C, d18O for heterogeneous samples/small samples may be larger.
Instrument:	Thermo Scientific MAT253 IRMS + Gasbench II
Operator:	Matteus Lindgren: matteus.lindgren@uit.no
Reference:	**Please add the following reference in publications based on this data** The Stable Isotope Laboratory at CAGE – Centre for Arctic Gas Hydrate, Environment and Climate located at UiT – The Arctic University of Norway, in Tromsø, Norway Website http://site.uit.no/sil/

Normalisation Standards

d13C	Standard 1	Standard 2	Standard 3	Comment
TRUE d13C [‰ vs VPDB]	1.96	-10.21	-48.95	
Normalised avg d13C this run [‰ vs VPDB]	1.87	-10.19	-48.96	
Standard deviation [‰ vs VPDB]	#DIV/0!	0.03	0.05	Spec. ≤0.10
Nr of replicates	1	7	4	

Linear regression R2-value d13C	1.00000	Spec. >0.99950

d18O	Standard 1	Standard 2	Standard 3	Comment
TRUE d18O [‰ vs VPDB]	-2.15	-18.59		
Normalised avg d18O this run [‰ vs VPDB]	-2.15	-18.59		
Standard deviation [‰ vs VPDB]	#DIV/0!	0.10		Spec. ≤0.10
Nr of replicates	1	7		

Linear regression R2-value d18O	0.99973	Spec. >0.99950

Quality Control Samples

d13C	QC Sample 1	QC Sample 2	Comment
TRUE d13C [‰ vs VPDB]	2.67	-46.60	
Normalised avg d13C this run [‰ vs VPDB]	#N/A	#N/A	
Standard deviation [‰ vs VPDB]	#N/A	#N/A	Spec. ≤0.10
Nr of replicates	0	0	

Samples

Sample name	Peak area [Vs]	d13C VPDB [‰]	d18O VPDB [‰]	Comment
50	46.48	-6.74	4.81	
49	37.11	-4.67	4.74	
48	28.53	-1.54	4.65	
47	118.87	-3.27	4.35	
46	21.54	-0.82	4.37	
45	41.85	-1.42	4.26	
44	40.15	-0.39	4.40	
43	35.87	-3.17	4.66	
42	39.75	-2.66	4.73	
41	35.26	-1.62	4.61	
40	33.32	-1.18	4.54	
39	45.25	-1.14	4.65	
38	34.81	-1.13	4.61	
37	41.86	-6.78	4.91	
36	30.91	-1.01	4.71	
35	43.40	-1.44	4.50	
34	30.67	-0.57	4.31	
33	29.64	-1.15	4.60	
32	32.21	-2.25	4.59	
31	30.22	-0.79	4.62	
30	34.42	-2.13	4.55	
29	45.05	-5.35	4.77	
28	42.50	-7.33	4.89	
27	33.56	-2.64	4.66	
26	33.51	-1.78	4.55	
25	28.12	-1.11	4.48	
24	30.91	-0.91	4.63	
23	57.29	-4.67	4.89	
22	29.25	-1.17	4.55	
21	26.67	-2.67	4.61	
1	55.20	-2.54	4.87	
2	34.11	-1.45	4.95	
3	52.97	-4.46	4.98	
4	36.48	-6.77	5.15	
5	43.72	-5.11	5.07	
6	26.03	-2.22	4.94	
7	39.19	-1.60	5.00	
8	50.43	-2.14	5.01	
9	54.29	-1.22	4.95	
10	43.58	-1.39	4.90	
11	47.01	-2.01	4.87	
12	47.68	-4.64	4.98	
13	43.62	-3.23	4.87	
14	22.91	-4.70	4.79	
15	31.97	-4.50	5.09	
16	31.85	-3.56	5.08	
17	34.14	-1.62	4.65	
18	66.59	-1.10	4.82	
19	25.96	-0.58	4.80	
20	34.04	-2.56	4.81	